Quantum Fisher information maximization in an unbalanced lossy interferometer

Stefan Ataman* and Karunesh K. Mishra

Extreme Light Infrastructure–Nuclear Physics (ELI-NP), "Horia Hulubei" National R&D Institute for Physics and Nuclear Engineering (IFIN-HH), 30 Reactorului Street, 077125 Măgurele, jud. Ilfov, Romania

(Received 27 February 2024; accepted 13 May 2024; published 11 June 2024)

In this work we address the problem of quantum Fisher information (QFI) maximization in an unbalanced lossy Mach-Zehnder interferometer. We implement the scheme from Escher *et al.* [Nat. Phys. **7**, 406 (2011)] allowing us to obtain in closed form the lossy QFI for all involved scenarios. Then, mirroring the lossless case Ataman [Phys. Rev. A **105**, 012604 (2022)], by optimizing the transmission coefficient of the first beam splitter, we maximize each QFI in question. We consider this problem for both single- and two-parameter QFI, i.e., for the scenarios with or without access to an external phase reference. Contrary to the lossless case, calculations are much more involved, however, we are able to put forward a large number of results in closed form. We also introduce two concepts, the balanced penalty and the QFI loss rate. Finally, we thoroughly discuss our results through a number of examples, including both Gaussian and non-Gaussian input states.

DOI: 10.1103/PhysRevA.109.062605

I. INTRODUCTION

Interferometry is a mature scientific field that provides measurement precision limited by the so-called shot-noise limit (SNL). Quantum interferometry [1,2] goes beyond the SNL and is able to reach the much more favorable Heisenberg limit (HL). As part of the emerging field of quantum sensing [3,4], interferometric quantum metrology is now both an active theoretical field of research as well as an applied technology allowing, for example, the detection of more gravitational wave events [5–9] or to enhance biological imaging [10–12].

Many workers in the field addressed the phase sensitivity of an interferometer [13–16] and the results are usually based on the error propagation formula. This phase sensitivity is detection scheme dependent and possibly suboptimal. One thus needs a tool to provide the theoretical optimal phase sensitivity. It turns out that the solution comes in the form of a lower bound based on the theoretical concept of Fisher information (FI) [17]. Indeed, the FI (denoted $F_{\rm cl}$) proved to be a theoretical tool of paramount importance in interferometric phase estimation [18–21] due to its connection to the Cramér-Rao bound (CRB), $\Delta\varphi_{\rm CRB} = 1/\sqrt{\mathcal{N}F_{\rm cl}}$, where $\mathcal{N}$ denotes the number of repeated measurements [22–24]. Its quantum counterpart, the quantum Fisher information (QFI) [19,25,26], $\mathcal{F}$, proved to be the perfect tool to evaluate the absolute best interferometric performance, optimized over all possible detection schemes [27]. Indeed, one can show that $\mathcal{F} \geqslant F_{\rm cl}$, hence the implied quantum Cramér-Rao bound (QCRB) $\Delta\varphi_{\rm QCRB} = 1/\sqrt{\mathcal{N}\mathcal{F}}$ [25,26] obeys $\Delta\varphi_{\rm QCRB} \leqslant \Delta\varphi_{\rm CRB}$. Readers interested in reviews on this topic can consult Refs. [27,28].

When considering a single phase shift (φ) inside the interferometer and boldly applying the QFI (denoted in this case $\mathcal{F}^{(i)}$), one gets a too optimistic result in terms of QCRB when compared to the actual achievable phase sensitivity for detection schemes not having access to an external phase reference (e.g., parity, difference intensity detection). This issue has been resolved in [29]. The authors pointed out that if the detection scheme does not have access to an external phase reference, the extra resources stemming from this availability have to be discounted. One is thus compelled to either average out the input state in respect with a common phase or use the two-parameter QFI (denoted here $\mathcal{F}^{(2p)}$) relevant for a difference-difference phase sensitivity. We will employ the latter option in this work. The same authors also considered the scenario with an external phase reference available and two antipodal internal phase shifts ($\pm\varphi/2$), the resulting QFI being denoted by $\mathcal{F}^{(ii)}$. We will discuss all three scenarios in this work.

One can thus ask the question if a balanced interferometer always maximizes the QFI in question. It turns out that if one is considering the two-parameter QFI $\mathcal{F}^{(2p)}$, then the answer is almost always positive [29–31]. However, if one considers scenarios where an external phase reference is available, then the opposite is true [31–33].

In the lossless case, balanced interferometers are commonplace in the literature, a fact often due to the use of detection schemes not having access to an external phase reference. In the lossy case, however, phase sensitivity optimization almost always goes via unbalancing, even for detection schemes not having access to an external phase reference, as already recognized by early papers dealing with this topic [34,35].

Although results have been reported in the literature for the lossy scenario [35–44], they are specifically optimized for a specific QFI setup (e.g., the two-parameter QFI) and a given input state (*e.g.,* coherent plus squeezed vacuum). Indeed,

*stefan.ataman@eli-np.ro

results have been reported for input states featuring a fixed number of input photons (e.g., Fock/NOON) [35–38]. The popular coherent plus squeezed vacuum [39,40,45] as well as the two-mode squeezed vacuum (TMSV) [39–41] input states have also been discussed in the literature. A special category of input states are the ones featuring one input port in the vacuum state [42,46,47]. Among them, we mention the results from [46] relative to a single squeezed vacuum input and the ones from Ref. [42] discussing a single coherent input.

Many authors considered unbalanced interferometers in the lossy case [34,37,42,45,46], thus providing the ultimate attainable precision in terms of phase sensitivity for their particular setup. However, other authors insisted on keeping the interferometer balanced [39,40,48,49]. As we will show in the following, this choice prevented them to obtain the true optimal QFI. A notable exception is the TMSV input state, where a balanced interferometer remains optimal in the lossy case, too [40,41,44]

A general scheme able to discuss QFI maximization in a lossy interferometer and with a generic input state, to the best of our knowledge, has not been put forward in the literature. The purpose of this work is to fill in this gap.

We employ the lossy QFI computation scheme introduced in [50] and obtain in closed form the lossy QFI for each scenario as well as the implied QCRB. Then, applying the same principles from the lossless case [31,32] and employing an unbalanced interferometer we optimize the transmission coefficient of the first beam splitter (denoted BS_1) in order to maximize each QFI in question.

As we will detail later, the single-parameter QFI $\mathcal{F}^{(i)}$ does not take into account losses in the arm not containing the phase shift. Thus, for a meaningful comparison of all involved schemes we only assume losses in the arm containing the phase shift, although for some specific cases we also give the results including losses in both arms.

This paper is organized as follows. In Sec. II the interferometric schemes we consider are put forward and some notation conventions are made. A very brief discussion of the QFI scenarios in the lossless case is done in Sec. III. The lossy QFI in each of the three considered scenarios is introduced and discussed in Sec. IV. The optimization of the transmission coefficient of BS_1 in the sense of maximizing each QFI in question is addressed in Sec. V. The discussed optimizations are applied to a number of Gaussian and non-Gaussian input states in Sec. VI. The conclusions from Sec. VII close the paper.

II. INTERFEROMETRIC SCHEME

In Fig. 1 we depict the interferometer scheme we consider. The Mach-Zehnder interferometer (MZI) comprises two beam splitters (BS_i with $i = 1, 2$) and the losses inside it are modeled via the fictitious beam spitters BS_{l2} (BS_{l3}) inserted in the upper (lower) arm featuring a transmission coefficient $\sqrt{\eta_1}$ ($\sqrt{\eta_2}$). For each interferometer arm, the lossless (total loss) case assumes $\eta_j = 1$ ($\eta_j = 0$), with $j = 2, 3$. The first beam splitter (BS_1) is assumed to be unbalanced and we model it via the unitary operator $\hat{U}_{\mathrm{BS}}(\vartheta) = e^{i\vartheta \hat{J}_x}$ [16] where the Schwinger pseudoangular momentum operators are defined as usual

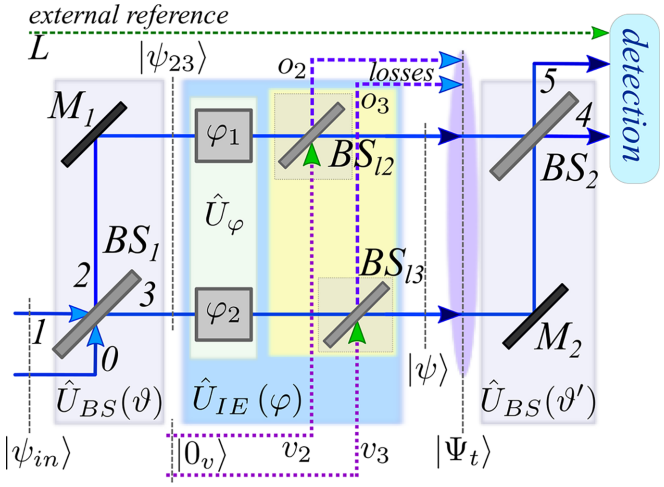

FIG. 1. The unbalanced MZI is composed of two beam splitters (BS_1 and BS_2) and two phase shifts (φ_1 and φ_2). Losses are modeled via the beam splitters BS_{l2} (BS_{l3}) in the upper (lower) arms having transmission coefficients $\sqrt{\eta_1}$ ($\sqrt{\eta_2}$).

by [51]

$$\hat{J}_x = \frac{\hat{a}_0^\dagger \hat{a}_1 + \hat{a}_0 \hat{a}_1^\dagger}{2}, \quad \hat{J}_y = \frac{\hat{a}_0^\dagger \hat{a}_1 - \hat{a}_0 \hat{a}_1^\dagger}{2i},$$
$$\hat{J}_z = \frac{\hat{a}_0^\dagger \hat{a}_0 - \hat{a}_1^\dagger \hat{a}_1}{2} \tag{1}$$

and the number operator for the input state is

$$\hat{N} = \hat{a}_0^\dagger \hat{a}_0 + \hat{a}_1^\dagger \hat{a}_1 = \hat{n}_0 + \hat{n}_1. \tag{2}$$

In the previous equations $\hat{a}_m$ ($\hat{a}_m^\dagger$) denote the usual annihilation (creation) operator and $\hat{n}_m$ denotes the photon number operator for mode m [52]. The abstract angle $\vartheta \in [0, \pi]$ is connected to the beam-splitter transmission coefficient T via the relation $\vartheta = 2 \arccos T$ and we consider a purely imaginary reflection coefficient $R = i \sin(\vartheta/2)$. Throughout this work, we will call a BS "balanced" if $T = 1/\sqrt{2}$ (i.e., $\vartheta = \pi/2$) and "degenerate" whenever we have $T = 0$ or 1. The variance of an operator $\hat{A}$ is defined as usual by $\Delta^2 \hat{A} = \langle \hat{A}^2 \rangle - \langle A \rangle^2$, the covariance of two operators $\hat{A}$ and $\hat{B}$ is defined via $\mathrm{Cov}(\hat{A}, \hat{B}) = \langle \hat{A}\hat{B} \rangle - \langle \hat{A} \rangle \langle \hat{B} \rangle$ while the symmetrized covariance of two noncommuting operators is

$$\widehat{\mathrm{Cov}}(\hat{A}, \hat{B}) = \frac{\langle \hat{A}\hat{B} \rangle + \langle \hat{B}\hat{A} \rangle}{2} - \langle \hat{A} \rangle \langle \hat{B} \rangle. \tag{3}$$

For future convenience, we also introduce Mandel's Q factor defined as [52]

$$Q_l = \frac{\Delta^2 \hat{n}_l - \langle \hat{n}_l \rangle}{\langle \hat{n}_l \rangle}, \tag{4}$$

where l denotes the mode in question. Expressing the field operators after BS_1 in respect with the input ones yields

$$\begin{cases} \hat{a}_2 = \cos\dfrac{\vartheta}{2}\hat{a}_0 + i \sin\dfrac{\vartheta}{2}\hat{a}_1 = T\hat{a}_0 + R\hat{a}_1, \\ \hat{a}_3 = i \sin\dfrac{\vartheta}{2}\hat{a}_0 + \cos\dfrac{\vartheta}{2}\hat{a}_1 = R\hat{a}_0 + T\hat{a}_1 \end{cases} \tag{5}$$

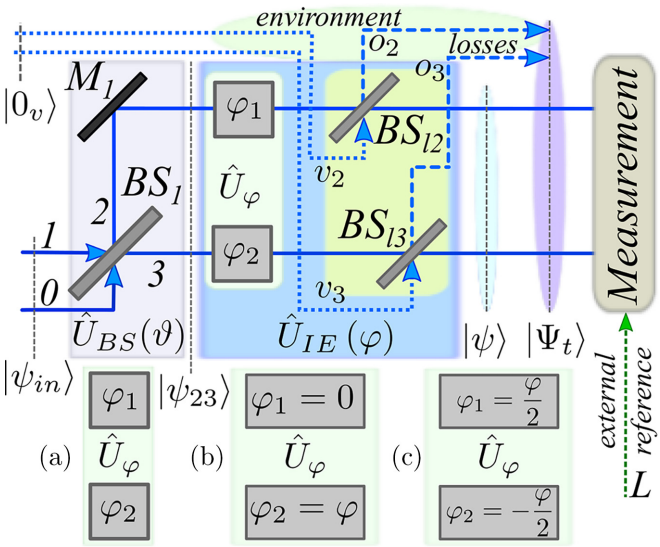

FIG. 2. The QFI schemes employed. For the two-parameter QFI evaluation, two independent phase shifts are assumed, as depicted in the upper drawing and also in lower drawing, case (a). For the asymmetric single-parameter QFI $\mathcal{F}^{(i)}$ the unitary operator modeling the phase shift is given by case (b). Finally, for the symmetric single-parameter QFI $\mathcal{F}^{(ii)}$, the unitary operator modeling the phase shift is given by case (c).

and from the previous equation we get the averages

$$\begin{cases} \langle \hat{n}_2 \rangle = \frac{1}{2}\langle \hat{N} \rangle - \sin\vartheta \langle \hat{J}_y \rangle + \cos\vartheta \langle \hat{J}_z \rangle, \\ \langle \hat{n}_3 \rangle = \frac{1}{2}\langle \hat{N} \rangle + \sin\vartheta \langle \hat{J}_y \rangle - \cos\vartheta \langle \hat{J}_z \rangle, \end{cases} \tag{6}$$

as well as the variances $\Delta^2\hat{n}_2$, $\Delta^2\hat{n}_3$ and the covariance $\mathrm{Cov}(\hat{n}_2, \hat{n}_3)$, given in Appendix A. We will employ in our calculations the relation

$$\Delta^2\hat{n}_2 + \Delta^2\hat{n}_3 + 2\,\mathrm{Cov}(\hat{n}_2, \hat{n}_3) = \Delta^2\hat{N}, \tag{7}$$

easily provable from the field operator transformations mentioned previously.

III. QFI IN THE LOSSLESS CASE AND ITS OPTIMIZATION

In this section we briefly discuss the lossless QFI case since these results will be needed when considering losses in Sec. IV. The second BS plays no role in the QFI calculation [21,32], hence we employ the simplified scheme from Fig. 2. In order to compute the QFI scenarios needed in this work [29,31,53], we first assume two independent phase shifts (φ_1 and φ_2, see Fig. 2) and perform the convenient variable change towards the sum and difference phases

$$\begin{cases} \varphi_s = \varphi_1 + \varphi_2, \\ \varphi_d = \varphi_1 - \varphi_2. \end{cases} \tag{8}$$

Introducing the generators $\hat{G}_s = (\hat{n}_2 + \hat{n}_3)/2$ and $\hat{G}_d = (\hat{n}_2 - \hat{n}_3)/2$ [29,32,53] allows us to write the wave vector after the phase shifts as $|\psi\rangle = \hat{U}_\varphi(\varphi_s, \varphi_d)|\psi_{23}\rangle$ where $|\psi_{23}\rangle = \hat{U}_{BS}(\vartheta)|\psi_{in}\rangle$ and the unitary operator modeling the phase shifts is

$$\hat{U}_\varphi(\varphi_s, \varphi_d) = e^{-i\varphi_s\hat{G}_s} e^{-i\varphi_d\hat{G}_d}. \tag{9}$$

We apply the usual formula for the Fisher matrix elements [29,53]

$$\mathcal{F}_{ij} = 4(\langle \hat{G}_i\hat{G}_j \rangle - \langle \hat{G}_i \rangle \langle \hat{G}_j \rangle), \tag{10}$$

where $i, j \in \{s, d\}$ and we denoted $\langle \hat{O} \rangle = \langle \psi | \hat{O} | \psi \rangle$. One ends up with the expressions

$$\begin{cases} \mathcal{F}_{ss} = 4\Delta^2\hat{G}_s = \Delta^2\hat{n}_2 + \Delta^2\hat{n}_3 + 2\,\mathrm{Cov}(\hat{n}_2, \hat{n}_3), \\ \mathcal{F}_{dd} = 4\Delta^2\hat{G}_d = \Delta^2\hat{n}_2 + \Delta^2\hat{n}_3 - 2\,\mathrm{Cov}(\hat{n}_2, \hat{n}_3), \\ \mathcal{F}_{sd} = 4\,\mathrm{Cov}(\hat{G}_s, \hat{G}_d) = \Delta^2\hat{n}_2 - \Delta^2\hat{n}_3. \end{cases} \tag{11}$$

When considering the scenario with a single internal phase shift [see Fig. 2(b)] we employ

$$\begin{cases} \varphi_1 = 0, \\ \varphi_2 = \varphi \end{cases} \tag{12}$$

while when we employ the $\pm\varphi/2$ convention [see Fig. 2(c)] we assume

$$\begin{cases} \varphi_1 = \frac{\varphi}{2}, \\ \varphi_2 = -\frac{\varphi}{2} \end{cases}. \tag{13}$$

As discussed previously [29,31,32], all QFI scenarios considered in this work can be constructed from the Fisher matrix elements given by Eq. (10). Thus, the two-parameter QFI, $\mathcal{F}^{(2p)}$, can be expressed as

$$\mathcal{F}^{(2p)} = \mathcal{F}_{dd} - \frac{\mathcal{F}_{sd}^2}{\mathcal{F}_{ss}} \tag{14}$$

valid when $\mathcal{F}_{ss} \neq 0$ and $\mathcal{F}^{(2p)} = \mathcal{F}_{dd}$ when $\mathcal{F}_{ss} = 0$. This QFI implies the difference-difference QCRB,

$$\Delta\varphi_{\mathrm{QCRB}}^{(2p)} = \frac{1}{\sqrt{\mathcal{N}\mathcal{F}^{(2p)}}}, \tag{15}$$

representing the "true" optimal interferometric phase sensitivity for a MZI with a detection scheme *not having access* to an external *phase reference* [29,31,32].

When an external phase reference is available and the convention (12) is assumed, the meaningful QFI is the asymmetric single-parameter QFI [31,32]

$$\mathcal{F}^{(i)} = \mathcal{F}_{ss} + \mathcal{F}_{dd} - 2\mathcal{F}_{sd} = 4\Delta^2\hat{n}_3 \tag{16}$$

and it implies the single-parameter QCRB [29]

$$\Delta\varphi_{\mathrm{QCRB}}^{(i)} = \frac{1}{\sqrt{\mathcal{N}\mathcal{F}^{(i)}}}. \tag{17}$$

Finally, when an external phase reference is available and the convention (13) is assumed the relevant QFI is the symmetric single-parameter QFI,

$$\mathcal{F}^{(ii)} = 4\Delta^2\hat{G}_d = \mathcal{F}_{dd}. \tag{18}$$

In respect with the input fields, the QFI from Eq. (14) can be written as

$$\mathcal{F}^{(2p)} = C_0 + C_1\frac{\sin^2\vartheta}{4} + C_2\frac{\sin 2\vartheta}{4} \tag{19}$$

and the C coefficients are given in Appendix B. The single-parameter asymmetric QFI given by Eq. (16) can be rewritten

as

$$\mathcal{F}^{(i)} = C_0' + \frac{\sin^2\vartheta}{4}C_1' + \frac{\sin 2\vartheta}{4}C_2' + \cos\vartheta C_3' + \frac{\sin\vartheta}{2}C_4', \tag{20}$$

where the C' coefficients are given in Appendix C. Finally, the single-parameter symmetric QFI from Eq. (18) can be expressed as

$$\mathcal{F}^{(ii)} = C_0'' + C_1''\frac{\sin^2\vartheta}{4} + C_2''\frac{\sin 2\vartheta}{4}, \tag{21}$$

where the coefficients are given by

$$\begin{cases} C_0'' = 4\Delta^2\hat{J}_z, \\ C_1'' = 16(\Delta^2\hat{J}_y - \Delta^2\hat{J}_z), \\ C_2'' = \widehat{\mathrm{Cov}}(\hat{J}_y, \hat{J}_z). \end{cases} \tag{22}$$

Details on the optimization of each QFI in question by adapting the BS_1 transmission coefficient $T = \cos\vartheta/2$ are found in [32] (see also the Supplemental Material [54]).

IV. QFI IN THE LOSSY CASE

We employ the general scheme of the lossy MZI scenario developed in Refs. [50,55] and details are given in Appendix D. Losses are modeled via fictitious beam splitters (see Fig. 1) with transmission (reflection) coefficients $T_{l_2} = \sqrt{\eta_1}$ ($R_{l_2} = \sqrt{1-\eta_1}$) in the upper arm and $T_{l_3} = \sqrt{\eta_2}$ ($R_{l_3} = \sqrt{1-\eta_3}$) in the lower one.

A. Fisher matrix elements

Following the same arguments employed in the lossless case (see Fig. 2 and Appendix D), we introduce the Fisher matrix elements:

$$\begin{cases} \mathcal{C}_{ss} = V_2\Delta^2\hat{n}_2 + V_3\Delta^2\hat{n}_3 + A_2\langle\hat{n}_2\rangle + A_3\langle\hat{n}_3\rangle \\ \qquad +V_{\mathrm{cov}}\mathrm{Cov}(\hat{n}_2,\hat{n}_3), \\ \mathcal{C}_{dd} = V_2\Delta^2\hat{n}_2 + V_3\Delta^2\hat{n}_3 + A_2\langle\hat{n}_2\rangle + A_3\langle\hat{n}_3\rangle \\ \qquad -V_{\mathrm{cov}}\mathrm{Cov}(\hat{n}_2,\hat{n}_3), \\ \mathcal{C}_{sd} = V_2\Delta^2\hat{n}_2 - V_3\Delta^2\hat{n}_3 + A_2\langle\hat{n}_2\rangle - A_3\langle\hat{n}_3\rangle, \end{cases} \tag{23}$$

where the coefficients are given by Eq. (E1), expressions that can be obtained from Eq. (D4), and by employing the Kraus operators (D6).

However, as we will point out in Sec. IV C, the single-parameter QFI has no dependence on η_1. In order to have a meaningful comparison among the single- and two-parameter QFI, in the following sections, starting from this point (unless otherwise specified) we will simplify our scheme so that we consider losses in the lower arm only (i.e., $\eta_1 = 1$). The coefficients from Eq. (E1) thus simplify to

$$\begin{cases} A_2 = 0, \\ A_3 = (\gamma_2+1)^2(1-\eta_2)\eta_2, \\ V_2 = 1, \\ V_3 = [1-(\gamma_2+1)(1-\eta_2)]^2, \\ V_{\mathrm{cov}} = 2[1-(\gamma_2+1)(1-\eta_2)]. \end{cases} \tag{24}$$

B. The scenario with no external phase reference available

Similar to the lossless case [31,32] (see also the Supplemental Material [54]) we define the difference-difference two-parameter QFI

$$\mathcal{C}^{(2p)} = \mathcal{C}_{dd} - \frac{\mathcal{C}_{sd}^2}{\mathcal{C}_{ss}} \tag{25}$$

valid for $\mathcal{C}_{ss} \neq 0$ and $\mathcal{C}^{(2p)} = \mathcal{C}_{dd}$ for $\mathcal{C}_{ss} = 0$, where the coefficients have been defined in Eq. (23). Since we employ the simplified scenario with losses in the lower arm only (i.e., $\eta_1 = 1$), by employing the coefficients from Eq. (24) we arrive at closed-form expression of the two-parameter QFI given in Appendix E, Eq. (E2). As pointed out in [50,55], the QFI $\mathcal{C}^{(2p)}$ is overoptimistic and the "true" lossy QFI is actually $\mathcal{G}^{(2p)} = \min_{\gamma_2}\{\mathcal{C}^{(2p)}\}$. One finds the optimum γ_2 value

$$\gamma_2^{\mathrm{opt}} = \frac{1}{1-\eta_2+\frac{\eta_2\langle\hat{n}_3\rangle(\Delta^2\hat{n}_2+\mathrm{Cov}(\hat{n}_2,\hat{n}_3))}{\Delta^2\hat{n}_2\Delta^2\hat{n}_3-[\mathrm{Cov}(\hat{n}_2,\hat{n}_3)]^2}} - 1 \tag{26}$$

that *minimizes* $\mathcal{C}^{(2p)}$ leading to the lossy two-parameter QFI,

$$\mathcal{G}^{(2p)} = \frac{\eta_2}{\frac{\eta_2}{\mathcal{F}^{(2p)}} + \frac{1-\eta_2}{4\langle\hat{n}_3\rangle}}. \tag{27}$$

From Eq. (27) one can immediately see the evolution of the lossy two-parameter QFI. Indeed, as $\eta_2 \to 1$ we have $\mathcal{G}^{(2p)} \to \mathcal{F}^{(2p)}$ while for the high-loss regime (i.e., $\eta_2 \ll 1-\eta_2$) the previous equation can be approximated to

$$\mathcal{G}^{(2p)} \approx \frac{4\eta_2}{1-\eta_2}\langle\hat{n}_3\rangle. \tag{28}$$

Finally, for total loss (i.e., $\eta_2 \to 0$) we have $\mathcal{G}^{(2p)} \to 0$.

Employing the QCRB $\Delta\varphi_{\mathrm{QCRB}}^{(2p)}$ from the lossless case given by Eq. (15) and the lossy QFI from Eq. (27) allows us to write the implied lossy QCRB as

$$\Delta\varphi_{\mathrm{QCRB}}^{(2p)}\big|_{\mathrm{lossy}} = \sqrt{\left[\Delta\varphi_{\mathrm{QCRB}}^{(2p)}\right]^2 + \frac{1-\eta_2}{\eta_2}[\Delta\varphi_{\mathrm{SNL}}]^2}, \tag{29}$$

where we defined the SNL-limited phase sensitivity $\Delta\varphi_{\mathrm{SNL}} = 1/\sqrt{4\mathcal{N}\langle\hat{n}_3\rangle}$. Thus, for η_2 close to 1 the first term from Eq. (29) dominates and we can approximate the QCRB with the lossless result from Eq. (15). As η_2 moves away from 1 the second term starts to be relevant and in the high-loss limit (i.e., $\eta_2 \ll 1-\eta_2$), the QFI can be approximated by Eq. (28) and we have

$$\Delta\varphi_{\mathrm{QCRB}}^{(2p)}\big|_{\mathrm{lossy}} \approx \sqrt{\frac{1-\eta_2}{\eta_2}}\Delta\varphi_{\mathrm{SNL}}. \tag{30}$$

C. The scenario with one phase shift and external phase reference available

Equation (16) remains valid in the lossy case, we thus have

$$\mathcal{C}^{(i)} = \mathcal{C}_{ss} + \mathcal{C}_{dd} - 2\mathcal{C}_{sd} \tag{31}$$

and considering losses in both arms, i.e., employing the coefficients from Eqs. (23) and (E1), we get the result (see also [50])

$$\mathcal{C}^{(i)} = 4(V_3\Delta^2\hat{n}_3 + A_3\langle\hat{n}_3\rangle) \tag{32}$$

and we have the important insight that the *losses in the upper arm* (i.e., in the arm without the phase shift) *are irrelevant* for the asymmetric single-parameter QFI, $\mathcal{C}^{(i)}$. Expanding the A_3 and V_3 coefficients yields

$$\mathcal{C}^{(i)} = 4[1-(\gamma_2+1)(1-\eta_2)]^2\Delta^2\hat{n}_3 + 4(\gamma_2+1)^2(1-\eta_2)\eta_2\langle\hat{n}_3\rangle \tag{33}$$

and the next step is to to minimize $\mathcal{C}^{(i)}$ in order to get the "true" QFI, i.e., $\mathcal{G}^{(i)} = \min_{\gamma_2}\{\mathcal{C}^{(i)}\}$. One finds [55]

$$\gamma_2^{\text{opt}} = \frac{\Delta^2\hat{n}_3}{(1-\eta_2)\Delta^2\hat{n}_3 + \eta_2\langle\hat{n}_3\rangle} - 1 \tag{34}$$

and replacing this result in the single-parameter QFI expression from Eq. (33) yields the asymmetric single-parameter lossy QFI [50],

$$\mathcal{G}^{(i)} = \frac{4\eta_2\langle\hat{n}_3\rangle\Delta^2\hat{n}_3}{\eta_2\langle\hat{n}_3\rangle + \Delta^2\hat{n}_3(1-\eta_2)}. \tag{35}$$

We can write the previous expression by employing the lossless QFI from Eq. (16) yielding the compact expression

$$\mathcal{G}^{(i)} = \frac{\eta_2}{\frac{\eta_2}{\mathcal{F}^{(i)}} + \frac{1-\eta_2}{4\langle\hat{n}_3\rangle}}. \tag{36}$$

Similar to Eq. (27), in the high-loss regime we find the scaling from Eq. (28) and for total loss we have $\mathcal{G}^{(i)} \to 0$.

Equally similar to the discussion from the previous section, we can write the lossy QCRB as

$$\Delta\varphi^{(i)}_{\text{QCRB}}\big|_{\text{lossy}} = \sqrt{\left[\Delta\varphi^{(i)}_{\text{QCRB}}\right]^2 + \frac{1-\eta_2}{\eta_2}[\Delta\varphi_{\text{SNL}}]^2}, \tag{37}$$

where the lossless QCRB $\Delta\varphi^{(i)}_{\text{QCRB}}$ is given by Eq. (17). It is noteworthy to point out that in this case, too, the QCRB in the high-loss regime is given by Eq. (30).

D. The scenario with two internal antisymmetrical phase shifts and external phase reference available

This scenario is depicted in Fig. 2(c) and the minimized symmetric single-parameter QFI is given in Appendix F. Since in the main text we assume losses in the lower arm only we impose $\eta_1 = 1$, thus, from Eqs. (F1) and (F3) we get the minimized symmetric single-parameter QFI

$$\mathcal{G}^{(ii)} = \frac{(1-\eta_2)\{\Delta^2\hat{n}_2\Delta^2\hat{n}_3 - [\text{Cov}(\hat{n}_2,\hat{n}_3)]^2\}}{(1-\eta_2)\Delta^2\hat{n}_3 + \eta_2\langle\hat{n}_3\rangle} + \frac{\eta_2[\Delta^2\hat{n}_2 + \Delta^2\hat{n}_3 - 2\text{Cov}(\hat{n}_2,\hat{n}_3)]\langle\hat{n}_3\rangle}{(1-\eta_2)\Delta^2\hat{n}_3 + \eta_2\langle\hat{n}_3\rangle}. \tag{38}$$

Contrary to the QFI in the other two scenarios, as $\eta_2 \to 0$ we arrive at a potentially non-null value,

$$\mathcal{G}^{(ii)}(0) = \Delta^2\hat{n}_2 - \frac{[\text{Cov}(\hat{n}_2,\hat{n}_3)]^2}{\Delta^2\hat{n}_3}. \tag{39}$$

This result can be explained by the fact that this time we have a phase shift in the upper arm, too, and since we assume losses in the lower one only, even for $\eta_2 \to 0$, information about φ can still be retrieved. Of course, assuming losses in both arms [see Eq. (F4) in Appendix F] and taking $\{\eta_1, \eta_2\} \to 0$ leads to $\mathcal{G}^{(ii)} \to 0$.

We can have a more compact form for the symmetric single-parameter QFI, namely,

$$\mathcal{G}^{(ii)} = \frac{(1-\eta_2)\mathcal{G}^{(ii)}(0)}{(1-\eta_2) + \frac{\eta_2\langle\hat{n}_3\rangle}{\Delta^2\hat{n}_3}} + \frac{\eta_2\mathcal{F}^{(ii)}}{\eta_2 + \frac{(1-\eta_2)\Delta^2\hat{n}_3}{\langle\hat{n}_3\rangle}}, \tag{40}$$

where the lossless QFI $\mathcal{F}^{(ii)}$ is given by Eq. (18) and we assumed $\{\langle\hat{n}_3\rangle, \Delta^2\hat{n}_3\} \neq 0$. This expression has also the advantage of making the limits $\eta_2 \to \{0, 1\}$ obvious.

In the case of a nonentangled BS_1 output [i.e., $\text{Cov}(\hat{n}_2, \hat{n}_3) = 0$] we have the much simpler expression

$$\mathcal{G}^{(ii)} = \Delta^2\hat{N} - \frac{(1-\eta_2)(\Delta^2\hat{n}_3)^2}{(1-\eta_2)\Delta^2\hat{n}_3 + \eta_2\langle\hat{n}_3\rangle}. \tag{41}$$

V. QFI MAXIMIZATION VIA BS_1 TRANSMISSION COEFFICIENT OPTIMIZATION IN THE LOSSY CASE

In this section we will derive the optimum transmission coefficients (denoted $T^{(2p)}_{\text{opt}}$, $T^{(i)}_{\text{opt}}$, and, respectively, $T^{(ii)}_{\text{opt}}$) in the sense that they maximize each QFI in question ($\mathcal{G}^{(2p)}$, $\mathcal{G}^{(i)}$, and, respectively, $\mathcal{G}^{(ii)}$). Since from this point on $\eta_1 = 1$, we will call η_2 the "loss coefficient" and the quantity $1-\eta_2$ the "loss rate."

A. Metrics quantifying the balanced and unbalanced interferometer performance

In order to quantify the effect of keeping the interferometer balanced (even if unbalancing it could yield an advantage), we introduce a metric applying to all three considered scenarios, which we call balanced QFI penalty or simply *balanced penalty*, defined via

$$\mathcal{P}(\eta_2) = \frac{\Delta\varphi_{\text{QCRB}}|_{\vartheta=\frac{\pi}{2}}}{\Delta\varphi_{\text{QCRB}}|_{\vartheta=\vartheta_{\text{opt}}}} = \sqrt{\frac{\mathcal{G}(\eta_2)|_{\vartheta=\vartheta_{\text{opt}}}}{\mathcal{G}(\eta_2)|_{\vartheta=\frac{\pi}{2}}}}, \tag{42}$$

where

$$\mathcal{G}(\eta_2)|_{\vartheta=\vartheta_{\text{opt}}} = \mathcal{G}_{\text{max}}(\eta_2) = \max_{\vartheta}\{\mathcal{G}(\eta_2)\}. \tag{43}$$

Here by $\mathcal{G}$ ($\mathcal{P}$) we understand one among $\mathcal{G}^{(i)}$ ($\mathcal{P}^{(i)}$), $\mathcal{G}^{(ii)}$ ($\mathcal{P}^{(ii)}$), and $\mathcal{G}^{(2p)}$ ($\mathcal{P}^{(2p)}$). The balanced penalty obeys $\mathcal{P}(\eta_2) \geqslant 1$ and can be seen as the degradation factor in terms of QCRB when one insists in keeping the interferometer balanced, no matter what. Having $\mathcal{P}(\eta_2) = 1$ implies that there is no interest in unbalancing the interferometer at a given loss coefficient η_2.

In order to better quantify the effect of loss, too, we introduce a metric for each QFI. For a given input state $|\psi_{\text{in}}\rangle$ and at a given loss rate η_2 we define the QFI loss rate by

$$\mathfrak{L}(\eta_2) = \frac{\max_{\vartheta}\{\mathcal{G}(\eta_2)\}}{\mathcal{F}_{\text{max}}}. \tag{44}$$

Here, too, by $\mathfrak{L}$ we understand one among $\mathfrak{L}^{(2p)}$, $\mathfrak{L}^{(i)}$, and $\mathfrak{L}^{(ii)}$ and correspondingly we have in Eq. (44) $\mathcal{G}^{(2p)}(\eta_2)$ and $\mathcal{F}^{(2p)}_{\text{max}}$, etc.

For $\eta_2 \to 1$ all QFI loss rates approach unity while for $\eta_2 \to 0$ both $\mathfrak{L}^{(i)}(\eta_2)$ and $\mathfrak{L}^{(2p)}(\eta_2)$ approach 0. This is not necessarily true for $\mathfrak{L}^{(ii)}(\eta_2)$.

B. The scenario when an external phase reference is unavailable

In this scenario the relevant QFI is the two-parameter one given by Eq. (27). When maximizing this QFI in respect with the transmission coefficient of BS_1, we find the following situations.

1. High-loss scenario

In the high-loss regime ($\eta_2 \ll 1-\eta_2$), from Eq. (28) we end up with the constraint $\langle \hat{n}_3\rangle' = 0$, i.e.,

$$\frac{\partial \langle \hat{n}_3\rangle}{\partial \vartheta} = 0. \tag{45}$$

One finds the solution

$$T_{\rm opt}^{(2p)} = \sqrt{\frac{1}{2} - \frac{\langle \hat{J}_z\rangle}{2\sqrt{\langle \hat{J}_y\rangle^2 + \langle \hat{J}_z\rangle^2}}} \tag{46}$$

valid if $\langle \hat{J}_z\rangle \neq 0$ and subject to the constraint $\langle \hat{J}_y\rangle > 0$ (i.e., it must be a maximum, not a minimum). In the case $\langle \hat{J}_y\rangle \leqslant 0$ one finds the degenerate solution

$$T_{\rm opt}^{(2p)} = \frac{1-{\rm sign}\langle \hat{J}_z\rangle}{2} \tag{47}$$

and if $\langle \hat{J}_z\rangle = 0$ we have $T_{\rm opt}^{(2p)} \in \{0,1\}$, i.e., both degenerate values yield the same maximum QFI.

2. Special case with one input in the vacuum state

In the scenario with one input port in the vacuum state [46] (i.e., $\langle \hat{n}_0\rangle = \Delta^2\hat{n}_0 = 0$) one finds the optimized two-parameter QFI

$$\mathcal{G}^{(2p)} = \frac{2\eta_2\langle \hat{n}_1\rangle \sin^2\vartheta}{1+\eta_2-(1-\eta_2)\cos\vartheta} \tag{48}$$

and for $\eta_2 \to 1$ (i.e., in the lossless case), as expected, the previous result morphs into the lossless result $\mathcal{F}^{(2p)} = \sin^2\vartheta\langle \hat{n}_1\rangle$ [32] (see also the Supplemental Material [54]). The QFI from Eq. (48) maximizes to

$$\mathcal{G}_{\rm max}^{(2p)} = \frac{4\eta_2\langle \hat{n}_1\rangle}{(1+\sqrt{\eta_2})^2} \tag{49}$$

by employing the optimum BS_1 transmission coefficient

$$T_{\rm opt}^{(2p)} = \sqrt{\frac{1}{1+\sqrt{\eta_2}}} \tag{50}$$

result also reported in Refs. [34,42]. The previous QFI leads to the QCRB (assuming a single measurement)

$$\Delta\varphi_{\rm SIL} = \frac{1+\sqrt{\eta_2}}{2\sqrt{\eta_2\langle \hat{n}_1\rangle}}. \tag{51}$$

This result is called SIL (standard interferometric limit) and was reported in Refs. [37,56,57].

Imposing BS_1 balanced modifies the QFI from Eq. (48) to $\mathcal{G}_{\rm bal}^{(2p)} = 2\eta_2\langle \hat{n}_1\rangle/(\eta_2+1)$ and the balanced penalty from definition (42) yields

$$\mathcal{P}^{(2p)}(\eta_2) = \frac{\sqrt{2(1+\eta_2)}}{1+\sqrt{\eta_2}}. \tag{52}$$

In the lossless case (i.e., $\eta_2 \to 1$) we find $\mathcal{P}^{(2p)} \to 1$ implying that there is no interest in unbalancing the interferometer for this scenario, as already discussed in the literature [32,46]. On the contrary, in the high-loss scenario there is a clear incentive to unbalance BS_1 since we find $\mathcal{P}^{(2p)} \to \sqrt{2}$.

The QFI loss rate defined by Eq. (44) is found to be

$$\mathfrak{L}^{(2p)}(\eta_2) = \frac{4\eta_2}{(1+\sqrt{\eta_2})^2}. \tag{53}$$

3. Case when the output of BS_1 is nonentangled

In the case of a nonentangled BS_1 output, the constraint $\partial\mathcal{G}^{(2p)}/\partial\vartheta = 0$ applied to Eq. (E3) leads us to the equation

$$\begin{aligned}&(1-\eta_2)\langle \hat{n}_3\rangle'(\Delta^2\hat{n}_2)^2(\Delta^2\hat{n}_3)^2\\&\quad+\eta_2\langle \hat{n}_3\rangle^2[(\Delta^2\hat{n}_2)^2-(\Delta^2\hat{n}_3)^2]\Delta^2\hat{n}_3' = 0.\end{aligned} \tag{54}$$

Further simplification is possible if both input states are coherent leading to the simple constraint from Eq. (45) implying the same conclusions from Sec. V B 1.

4. General case

The formal solution can be obtained from Eq. (27) by differentiating it in respect with ϑ and we have

$$\begin{aligned}&(1-\eta_2)\langle \hat{n}_3\rangle'(\Delta^2\hat{n}_2\Delta^2\hat{n}_3-[{\rm Cov}(\hat{n}_2,\hat{n}_3)]^2)^2\\&\quad+\eta_2\langle \hat{n}_3\rangle^2(\Delta^2\hat{n}_2\Delta^2\hat{n}_3-[{\rm Cov}(\hat{n}_2,\hat{n}_3)]^2)'\Delta^2\hat{N} = 0.\end{aligned} \tag{55}$$

Equation (55) reexpressed in respect with the input variables via Eqs. (6) and (A1) yields a polynomial equation in ϑ. Among the solutions $\vartheta_{\rm sol}^{(2p)}$ of this equation one finds the optimum $\vartheta_{\rm opt}^{(2p)}$ that maximizes the QFI $\mathcal{G}^{(2p)}$. For a similar calculation, see the Supplemental Material [54].

C. Scenario with a single-phase internal shift and external phase reference available

In this scenario the relevant QFI is the asymmetric single-parameter one given by Eq. (35). When maximizing this QFI in respect with the transmission coefficient of BS_1, we find the following situations.

1. High-loss scenario

In the high-loss limit we find the constraint $\langle \hat{n}_3\rangle' = 0$ and all results from Sec. V B apply.

2. Special case with one input in the vacuum state

For the special case with one input in the vacuum state the QFI from Eq. (35) becomes

$$\mathcal{G}^{(i)} = \frac{4\eta_2\cos^2\frac{\vartheta}{2}\langle \hat{n}_1\rangle\left(\sin^2\frac{\vartheta}{2}\langle \hat{n}_1\rangle+\cos^2\frac{\vartheta}{2}\Delta^2\hat{n}_1\right)}{\eta_2\langle \hat{n}_1\rangle+(1-\eta_2)\left(\sin^2\frac{\vartheta}{2}\langle \hat{n}_1\rangle+\cos^2\frac{\vartheta}{2}\Delta^2\hat{n}_1\right)}. \tag{56}$$

We are ready now to find the needed optima as well as the balanced penalties. We have the following:

(i) if $Q_1 \geqslant -\frac{1}{1+\sqrt{\eta_2}}$ the optimal transmission coefficient is $T_{\rm opt}^{(i)} = 1$, yielding the maximum QFI

$$\mathcal{G}_{\rm max}^{(i)} = \frac{4\eta_2\langle\hat{n}_1\rangle(Q_1+1)}{(1-\eta_2)Q_1+1} \tag{57}$$

and, as $\eta_2 \to 1$ the condition becomes $Q_1 \geqslant -0.5$ with the previous QFI migrating into the lossless result [32] (see also the Supplemental Material [54]). The balanced penalty is found to be

$$\mathcal{P}^{(i)} = \sqrt{\frac{2(Q_1+1)[(1-\eta_2)Q_1+2]}{(Q_1+2)[(1-\eta_2)Q_1+1]}}. \tag{58}$$

(ii) if $Q_1 < -\frac{1}{1+\sqrt{\eta_2}}$ the optimal transmission coefficient is

$$T_{\rm opt}^{(i)} = \sqrt{-\frac{1}{Q_1(\sqrt{\eta_2}+1)}} \tag{59}$$

leading to the maximum QFI

$$\mathcal{G}_{\rm max}^{(i)} = -\frac{4\langle\hat{n}_1\rangle\eta_2}{(\sqrt{\eta_2}+1)^2 Q_1}. \tag{60}$$

The limit $\eta_2 \to 1$ morphs $\mathcal{G}_{\rm max}^{(i)}$ into its lossless counterpart $\mathcal{F}_{\rm max}^{(i)}$ (see the Supplemental Material [54]). This time we end up with the balanced penalty

$$\mathcal{P}^{(i)} = \sqrt{-\frac{2[(1-\eta_2)Q_1+2)]}{(\sqrt{\eta_2}+1)^2 Q_1(Q_1+2)}}. \tag{61}$$

3. Case when $C_2' = C_4' = 0$

If the input state obeys $\langle\hat{a}_0\rangle = 0$ implying the constraints $C_2' = C_4' = 0$, we find the optimum transmission coefficient of BS_1 by solving the equation

$$\mathcal{A}_4 y^4 + \mathcal{A}_3 y^3 + \mathcal{A}_2 y^2 + \mathcal{A}_1 y + \mathcal{A}_0 = 0, \tag{62}$$

where $\vartheta_{\rm sol} = \arccos y$, and the $\mathcal{A}_0 - \mathcal{A}_4$ coefficients are given in Appendix G. Among the solutions $\vartheta_{\rm sol}$ of this equation we find the value $\vartheta_{\rm opt}^{(i)}$ that maximizes the single-parameter QFI from Eq. (35).

Given an input state obeying the constraints $C_2' = C_4' = 0$ and yielding nondegenerate optimum $\vartheta_{\rm opt}^{(i)}$ in the lossless case [32] (see details also in the Supplemental Material [54]), we can also ask the following question: What maximum losses $\eta_{2\rm lim}$ can be allowed, so that the implied lossy optimum from Eq. (62) is *not* degenerate? One finds the answer:

$$\eta_{2\rm lim} \geqslant \frac{\langle\hat{J}_z\rangle}{\langle\hat{J}_z\rangle + \frac{-2C_1'+4C_3'}{(C_0'+C_3')^2}\langle\hat{n}_1\rangle^2}. \tag{63}$$

4. General case

Starting with Eq. (35) and imposing the constraint $\partial\mathcal{G}^{(i)}/\partial\vartheta = 0$ leads to

$$(1-\eta_2)(\langle\hat{n}_3\rangle)'(\Delta^2\hat{n}_3)^2 + \eta_2\langle\hat{n}_3\rangle^2(\Delta^2\hat{n}_3)' = 0, \tag{64}$$

where we recall that by $(\ldots)'$ we understand $\partial(\ldots)/\partial\vartheta$. In the lossless limit $\eta_2 \to 1$, we recover the already reported results [31,32] (see also the Supplemental Material [54]).

By employing Eqs. (6) and (A1) we are able to write the constraint from Eq. (64) in respect with ϑ. We end up with a 10th-degree equation and among the solutions we find $\vartheta_{\rm opt}$ that maximizes the asymmetric single-parameter QFI to $\mathcal{G}_{\rm max}^{(i)}$. Details are found in the Supplemental Material [54].

D. Scenario with two antisymmetric phase shifts and external phase reference available

In this scenario the relevant QFI is the symmetric single-parameter one given by Eq. (38). When maximizing this QFI in respect with the transmission coefficient of BS_1, we find the following situations.

1. High-loss scenario

In the high-loss scenario (i.e., $\eta_2 \ll 1-\eta_1$) from Eq. (39) we get the formal constraint

$$[\mathrm{Cov}(\hat{n}_2,\hat{n}_3)(\Delta^2\hat{n}_3)' + \Delta^2\hat{n}_3(\Delta^2\hat{n}_2)'] \times (\Delta^2\hat{n}_3 + \mathrm{Cov}(\hat{n}_2,\hat{n}_3)) = 0 \tag{65}$$

and solutions to this equation are given in Appendix H.

2. Special case with one input in the vacuum state

With port 0 kept in the vacuum state, the expression of the symmetric single-parameter QFI is found to be

$$\mathcal{G}^{(ii)} = \langle\hat{n}_1\rangle\frac{2\eta_2(\cos^2\vartheta Q_1+1)}{(1-\eta_2)(1+\cos\vartheta)Q_1+2} + \langle\hat{n}_1\rangle\frac{(1-\cos\vartheta)(1-\eta_2)(Q_1+1)}{(1-\eta_2)(1+\cos\vartheta)Q_1+2}. \tag{66}$$

In the lossless case ($\eta_2 \to 1$), as expected, we stumble upon the already reported result [32]

$$\mathcal{F}^{(ii)} = \cos^2\vartheta(\Delta^2\hat{n}_1 - \langle\hat{n}_1\rangle) + \langle\hat{n}_1\rangle. \tag{67}$$

When optimizing the QFI $\mathcal{G}^{(ii)}$ for the scenario with input port 0 left in the vacuum state we find two cases.

(i) If $Q_1 < \frac{\sqrt{\eta_2}-1}{\sqrt{\eta_2}+1}$ we find the optimum transmission coefficient

$$T_{\rm opt}^{(ii)} = \sqrt{\frac{Q_1+1+\sqrt{\eta_2}(Q_1-1)}{2(\eta_2+\sqrt{\eta_2})Q_1}} \tag{68}$$

leading to the maximum symmetric single-parameter QFI

$$\mathcal{G}_{\rm max}^{(ii)} = \frac{\langle\hat{n}_1\rangle[\eta_2(3Q_1-1)+(Q_1+1)(2\sqrt{\eta_2}-1)]}{(\sqrt{\eta_2}+1)^2 Q_1} \tag{69}$$

and we find a balanced penalty

$$\mathcal{P}^{(ii)}(\eta_2) = \left([2+(1-\eta_2)Q_1] \times \frac{(2\sqrt{\eta_2}-1)(Q_1+1)+\eta_2(3Q_1-1)}{(\sqrt{\eta_2}+1)^2 Q_1(1+\eta_2-(1-\eta_2)Q_1)}\right)^{\frac{1}{2}}. \tag{70}$$

(ii) Finally, if $Q_1 \geqslant \frac{\sqrt{\eta_2}-1}{\sqrt{\eta_2}+1}$ the optimum transmission coefficient is found in the degenerate case $T_{\rm opt}^{(ii)} = 0$ leading to the

optimum lossy QFI $\mathcal{G}^{(ii)}_{\max} = \Delta^2\hat{n}_1$ and we have the balanced penalty

$$\mathcal{P}^{(ii)}(\eta_2) = \sqrt{2 + Q_1 - \frac{2\eta_2}{\eta_2(1-Q_1)+Q_1+1}}. \tag{71}$$

In the high-loss limit (irrespective on the value of Q_1) we find $T^{(ii)}_{\text{opt}} \to 0$ and $\mathcal{G}^{(ii)}_{\max} \to \Delta^2\hat{n}_1$, leading to a balanced penalty

$$\mathcal{P}^{(ii)}(\eta_2 \to 0) = \sqrt{2+Q_1} \tag{72}$$

and the only situation when unbalancing the interferometer is not interesting happens for $Q_1 = -1$.

3. *Case when the output of BS$_1$ is unentangled*

The special case when $\text{Cov}(\hat{n}_2, \hat{n}_3) = 0$ leads to a simpler result, namely,

$$((1-\eta_2)\Delta^2\hat{n}_3 + 2\eta_2\langle\hat{n}_3\rangle)(\Delta^2\hat{n}_3)' - \eta_2\Delta^2\hat{n}_3\langle\hat{n}_3\rangle' = 0 \tag{73}$$

leading to Eq. (H4) discussed in Appendix H.

4. *General case*

The equation yielding the formal solution for the optimum $T^{(ii)}_{\text{opt}}$ in the general case is found in Appendix H.

VI. RESULTS FOR A NUMBER OF GAUSSIAN AND NON-GAUSSIAN INPUT STATES

In this section we apply the results presented up to this point to a number of input states having a practical interest. These are the double coherent input state [31,58,59] due to its semiclassical nature and the practical interest of its limiting case of single coherent input [42,60]; the coherent plus squeezed vacuum input for is broad and diverse uses [7,8,15,60]; the coherent plus Fock input for its interest in quantum metrology [61–63], the double Fock input for fixed-photon number metrology and NOON state interferometry [35,64]; finally, the TMSV input state for its interest in metrology [63,65] and optical quantum communications [66,67].

A. Double coherent input state

Let us consider the double coherent input state [58,59]

$$|\psi_{\text{in}}\rangle = |\alpha_1\beta_0\rangle = \hat{D}_1(\alpha)\hat{D}_0(\beta)|0_1 0_0\rangle. \tag{74}$$

A coherent state is obtained via the displacement or Glauber operator [52,68,69]

$$\hat{D}_k(\kappa) = e^{\kappa\hat{a}_k^\dagger - \kappa^*\hat{a}_k} \tag{75}$$

with $k = 1, 0$ and $\kappa = \alpha, \beta$. For the input port 1 (0) we thus have $\alpha = |\alpha|e^{i\theta_\alpha}$ ($\beta = |\beta|e^{i\theta_\beta}$). The input PMC is given by $\Delta\theta = \theta_\alpha - \theta_\beta$. We denote the coherent amplitude ratio by $\varpi = |\beta|/|\alpha|$ [59] and throughout this section we assume $\alpha \neq 0$.

We start with the two-parameter QFI, $\mathcal{G}^{(2p)}$. Its expression is given in Appendix I, Eq. (I1). The optimum BS$_1$ transmission coefficient that maximizes $\mathcal{G}^{(2p)}$ is found to be

$$T^{(2p)}_{\text{opt}} = \sqrt{\frac{1}{1+\tan^2\left(\frac{\vartheta^{(2p)}_{\text{opt}}}{2}\right)}}, \tag{76}$$

where $\vartheta^{(2p)}_{\text{opt}}$ is given in Eq. (I2).

For the scenario comprising a single internal phase shift and an external phase reference available, Eq. (16) is relevant in the lossless case and one finds the optimum transmission coefficient

$$T^{(i)}_{\text{opt}} = \frac{1}{\sqrt{2}}\sqrt{1 + \frac{1-\varpi^2}{\sqrt{1+2\varpi^2(2\sin^2\Delta\theta - 1)+\varpi^4}}} \tag{77}$$

if $\sin\Delta\theta > 0$ and $T^{(i)}_{\text{opt}} = [1 - \text{sign}(\varpi - 1)]/2$ if $\sin\Delta\theta \leqslant 0$. The maximum QFI is found to be

$$\mathcal{F}^{(i)}_{\max} = 2|\alpha|^2\left(1 + \varpi^2 + \sqrt{(1-\varpi^2)^2 + 4\varpi^2\sin^2\Delta\theta}\right). \tag{78}$$

The previous expression obviously maximizes for the input phase matching condition (PMC) $\sin\Delta\theta = 1$ (see the discussion from Ref. [31]) yielding the maximum obtainable QFI for a double coherent input state $\mathcal{F}^{(i)}_{\max} = 4(|\alpha|^2 + |\beta|^2)$. For the same scenario in the lossy case, since $\Delta^2\hat{n}_3 = \langle\hat{n}_3\rangle$, from Eq. (35) one finds

$$\mathcal{G}^{(i)} = \eta_2\mathcal{F}^{(i)} = 4\eta_2\langle\hat{n}_3\rangle \tag{79}$$

implying QFI loss rate

$$\mathfrak{L}^{(i)} = \eta_2. \tag{80}$$

Two conclusions are immediate: (i) the optimum transmission coefficient $T^{(i)}_{\text{opt}}$ is identical to the one found in the lossless case [see Eq. (77)] and (ii) the losses in terms of phase sensitivity scale as $1/\sqrt{\eta_2}$, a result expected for coherent states [57].

For the scenario with two $\pm\varphi/2$ internal phase shifts and external phase reference available, one finds the lossless QFI [31]

$$\mathcal{F}^{(ii)} = |\alpha|^2 + |\beta|^2 \tag{81}$$

and this result holds *irrespective* on the value of the transmission coefficient of BS$_1$. In the lossy case one finds

$$\mathcal{G}^{(ii)} = (1-\eta_2)\Delta^2\hat{n}_2 + \eta_2(|\alpha|^2 + |\beta|^2) \tag{82}$$

and the same result expressed in respect with the input variables is given in Eq. (I3). An optimum transmission coefficient $T^{(ii)}_{\text{opt}}$ maximizing this QFI can be found (see Appendix I) and the value $\mathcal{G}^{(ii)}_{\max}$ is given in Eq. (I5). An interesting scenario appears if we impose the input PMC $\sin\Delta\theta = -1$. From Eq. (I4) we get

$$T^{(ii)}_{\text{opt}} = \sqrt{\frac{1}{2} + \frac{|1-\varpi^2|\text{sign}(1-\varpi)}{2(1+\varpi^2)}} \tag{83}$$

and the maximum QFI from Eq. (I5) becomes

$$\mathcal{G}^{(ii)} = |\alpha|^2 + |\beta|^2 = |\alpha|^2(1+\varpi^2), \tag{84}$$

i.e., it becomes *independent* of the loss coefficient η_2 and equals the lossless QFI from Eq. (81). Thus, contrary to the QFI $\mathcal{G}^{(i)}$, we now have a QFI loss rate

$$\mathfrak{L}^{(ii)} = 1, \tag{85}$$

i.e., total immunity to losses.

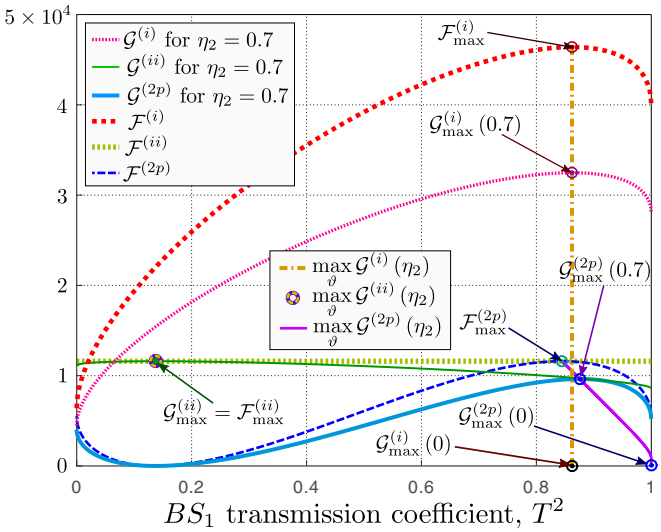

FIG. 3. The three considered QFI scenarios versus the transmission coefficient of BS_1 for a double coherent input state. Their respective maxima for $\eta_2 \in [0, 1]$ are also plotted. Parameters used: $|\alpha| = 10^2$, $|\beta| = 40$. The PMC $\Delta\theta = -\frac{\pi}{2}$ was employed for $\mathcal{G}^{(ii)}$ and $\mathcal{G}^{(2p)}$ and the PMC $\Delta\theta = \frac{\pi}{2}$ for $\mathcal{G}^{(i)}$.

In Fig. 3 we plot all three QFI scenarios versus the transmission coefficient of BS_1. For the scenario not having access to an external phase reference, $\mathcal{F}^{(2p)}$ (dashed blue curve) leads to a maximum QFI (see Refs. [31,32])

$$\mathcal{F}^{(2p)}_{\max} = |\alpha|^2 + |\beta|^2. \tag{86}$$

For the lossy case (thick solid light-blue curve) we have an optimum $T^{(2p)}_{\text{opt}}$ derived in Appendix I and as $\eta_2 \to 0$ the limit from Eq. (46) applies and we get $T^{(2p)}_{\text{opt}} \to 1$.

For the scenario having access to an external phase reference, as previously discussed in the literature [31], $\mathcal{F}^{(i)}$ maximizes for the input PMC $\Delta\theta = \pi/2$ (thick dotted red curve) and the optimum BS_1 leading to its maximum value is given by Eq. (38) from Ref. [32]. The lossy case QFI $\mathcal{G}^{(i)}$ (pink dotted curve) is given by Eq. (79) and it maximized by the same $T^{(i)}_{\text{opt}}$ from the lossless case.

For the scenario with two internal $\pm\varphi/2$ phases and external phase reference available, the QFI $\mathcal{F}^{(ii)}$ (thick light-green horizontal dashed curve) is insensitive to the transmission coefficient of BS_1. This result does not hold anymore for $\mathcal{G}^{(ii)}$ (thin solid green curve), however, as previously mentioned, for the input PMC $\Delta\theta = -\frac{\pi}{2}$, irrespective on the value of η_2, fixing T to the value $T^{(ii)}_{\text{opt}}$ given by Eq. (83) leads to the surprising result that the maximum QFI is immune to losses, i.e., $\mathcal{G}^{(ii)}_{\max} = \mathcal{F}^{(ii)}$.

B. Coherent plus squeezed vacuum input state

Let us consider now the widely used coherent plus squeezed vacuum input state [52,60,70,71]

$$|\psi_{\text{in}}\rangle = |\alpha_1 \xi_0\rangle, \tag{87}$$

where $|\xi_0\rangle = \hat{S}_0(\xi)|0_0\rangle$ and the squeezing operator is

$$\hat{S}_0(\xi) = e^{\frac{1}{2}[\xi^* \hat{a}_0^2 - \xi (\hat{a}_0^\dagger)^2]} \tag{88}$$

with $\xi = re^{i\theta}$. Throughout this section, we assume that the optimum input PMC $2\theta_\alpha - \theta = 0$ is always satisfied [60,71].

In the lossless case, the two-parameter QFI is given by

$$\mathcal{F}^{(2p)} = \sin^2\vartheta(|\alpha|^2 e^{2r} + \sinh^2 r) + \frac{4\cos\vartheta|\alpha|^2 \sinh^2 2r}{2|\alpha|^2 + \sinh^2 2r} \tag{89}$$

and it maximizes in the balanced case [29,31] yielding the well-known result $\mathcal{F}^{(2p)}_{\max} = |\alpha|^2 e^{2r} + \sinh^2 r$ [53,60]. From Eq. (6) we have the average value of the number of photons,

$$\langle \hat{n}_3 \rangle = |\alpha|^2(1 + \cos\vartheta) + \sinh^2 r(1 - \cos\vartheta), \tag{90}$$

and inserting the previous two results into Eq. (27) yields the lossy two-parameter QFI, $\mathcal{G}^{(2p)}$. If we insist on force balancing BS_1, we end up with the result

$$\mathcal{G}^{(2p)}_{\text{bal}} = \frac{2\eta_2(|\alpha|^2 e^{2r} + \sinh^2 r)}{2\eta_2 + (1-\eta_2)\frac{|\alpha|^2 e^{2r} + \sinh^2 r}{|\alpha|^2 + \sinh^2 r}} \tag{91}$$

and, as we will discuss shortly, this QFI is not optimal (except when $\eta_2 = 1$).

In the high-coherent regime (i.e., for $|\alpha|^2 \gg \sinh^2 r$) we can approximate the two-parameter lossy QFI to

$$\mathcal{G}^{(2p)} \approx \frac{2\eta_2|\alpha|^2 e^{2r}\sin^2\vartheta(1+\cos\vartheta)}{2\eta_2(1+\cos\vartheta) + (1-\eta_2)\sin^2\vartheta e^{2r}} \tag{92}$$

and the optimum transmission coefficient maximizing this QFI is found to be

$$T^{(2p)}_{\text{opt}} \approx \sqrt{1 + \frac{\sqrt{\eta_2}e^{-r}(\sqrt{\eta_2}e^{-r} - \sqrt{1-\eta_2(1-e^{-2r})})}{(1-\eta_2)}}. \tag{93}$$

Balancing BS_1 brings the result from Eq. (92) to

$$\mathcal{G}^{(2p)} \approx \frac{2\eta_2|\alpha|^2}{1 - \eta_2 + 2\eta_2 e^{-2r}}. \tag{94}$$

Moving on to the asymmetric single-parameter QFI, in the lossless case it is found to be [29,31,40]

$$\mathcal{F}^{(i)} = 2\sin^4\frac{\vartheta}{2}\sinh^2 2r + 4\cos^4\frac{\vartheta}{2}|\alpha|^2 + \sin^2\vartheta(\sinh^2 r + |\alpha|^2 e^{2r}). \tag{95}$$

Using this result and $\langle \hat{n}_3 \rangle$ from Eq. (90), we easily obtain the lossy single-parameter QFI via Eq. (36). In the high-coherent regime ($|\alpha|^2 \gg \sinh^2 r$) we have the approximation

$$\mathcal{G}^{(i)} \approx \frac{4\eta_2|\alpha|^2\cos^2\left(\frac{\vartheta}{2}\right)}{1 - \frac{2\eta_2 \sinh r \sin^2\left(\frac{\vartheta}{2}\right)}{\cosh r - \sinh r\cos\vartheta}}. \tag{96}$$

In this regime, an optimum BS_1 transmission coefficient $T^{(i)}_{\text{opt}}$ maximizing the previous QFI to $\mathcal{G}^{(i)}_{\max}$ can be obtained in

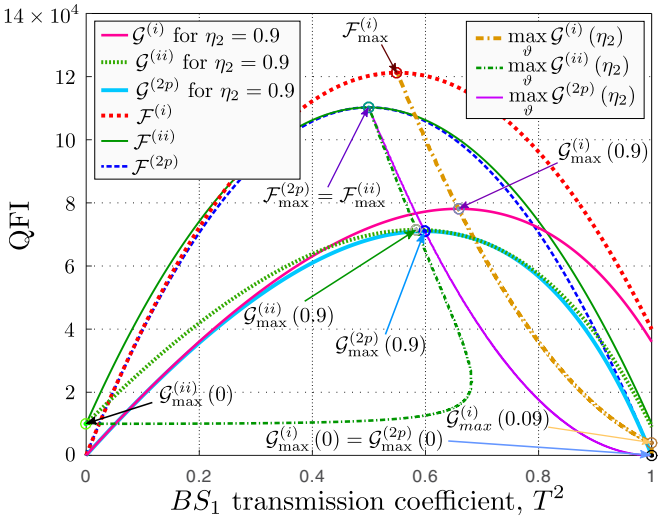

FIG. 4. The three QFI scenarios versus the transmission coefficient of BS_1 in the lossy scenario for a coherent plus squeezed vacuum input state. Their respective maxima for $\eta_2 \in [0, 1]$ are also plotted. Parameters used: $|\alpha| = 10^2$, $r = 1.2$, PMC $2\theta_\alpha - \theta = 0$.

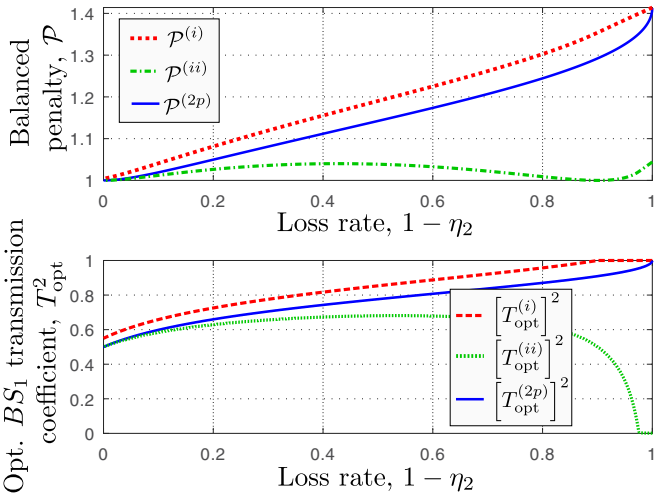

FIG. 5. The balanced penalties for a coherent plus squeezed vacuum input state (upper subfigure) and the corresponding transmission coefficients (lower subfigure) versus the loss rate $1 - \eta_2$. Parameters used: $|\alpha| = 10^2$, $r = 1.2$, PMC $2\theta_\alpha - \theta = 0$.

closed form and these results are given in Appendix J. Balancing BS_1 modifies (96) to

$$\mathcal{G}^{(i)}_{\text{bal}} \approx \frac{4\eta_2|\alpha|^2 \cosh r}{\cosh r - 2\eta_2 \sinh r}, \tag{97}$$

a result that can be related[1] to the one reported in Ref. [40]. Similar to the two-parameter QFI case, the force-balanced asymmetric single-parameter QFI is not optimal.

The lossless symmetric single-parameter QFI is

$$\mathcal{F}^{(ii)} = \sin^2\vartheta(\sinh^2 r + |\alpha|^2 e^{2r}) + \cos^2\vartheta\left(\frac{\sinh^2 2r}{2} + |\alpha|^2\right) \tag{98}$$

and its maximum $\mathcal{F}^{(ii)}_{\max} = \sinh^2 r + |\alpha|^2 e^{2r}$ is reached in the balanced case. Using the previous result and employing Eq. (40) yields the lossy $\mathcal{G}^{(ii)}$. In the high-coherent approximation the optimum BS_1 transmission coefficient is found to be

$$T^{(ii)}_{\text{opt}} = \sqrt{1 + \frac{2\sqrt{\eta_2}e^{-r} - (1+\eta_2)\sqrt{1-\eta_2(1-e^{-2r})}}{4(1-\eta_2)\sqrt{\eta_2}\sinh r}} \tag{99}$$

valid for $\eta_2 \neq 0$ and $r > \log\sqrt{(1+3\eta_2)/4\eta_2}$. Replacing $T^{(ii)}_{\text{opt}}$ into the QFI leads to its maximum value given by Eq. (J3).

In Fig. 4 we depict the scenarios for each aforementioned QFI in respect with the transmission coefficient of BS_1. The lossless two-parameter QFI $\mathcal{F}^{(2p)}$ (dashed blue curve), as discussed previously [29,31], maximizes in the balanced case. For the considered input parameters, its lossy counterpart $\mathcal{G}^{(2p)}$ (solid light-blue curve for $\eta_2 = 0.9$) maximizes for values $T^{(2p)}_{\text{opt}}$ above $\sqrt{0.5}$ and as losses increase $T^{(2p)}_{\text{opt}} \to 1$. The evolution of $\mathcal{G}^{(2p)}_{\max}(\eta_2)$ as η_2 goes from 1 to 0 is depicted by the solid magenta curve.

The asymmetric single-parameter QFI $\mathcal{F}^{(i)}$ (thick dotted red curve) maximizes in the unbalanced case ($T^{(i)}_{\text{opt}} \approx \sqrt{0.54}$ for our parameters) yielding $\mathcal{F}^{(i)}_{\max} \approx 12.1\times10^4$. Its lossy counterpart $\mathcal{G}^{(i)}$ (depicted as a thick solid pink curve for $\eta_2 = 0.9$) continues this trend, e.g., for $\eta_2 = 0.9$ one finds $T^{(i)}_{\text{opt}} \approx \sqrt{0.66}$. $T^{(i)}_{\text{opt}}$ actually reaches 1 for the limit loss value $\eta_{2\text{lim}} = 0.09$ as given by Eq. (63) and for any value $\eta_2 \leqslant \eta_{2\text{lim}}$ we have $T^{(i)}_{\text{opt}} = 1$.

We also plot in Fig. 4 the evolution of the maximum lossy QFI $\mathcal{G}^{(i)}_{\max}(\eta_2)$ for each η_2 from 1 down to 0 (thick dashed-dotted orange curve). One remarks that, compared to $\mathcal{G}^{(2p)}$, $\mathcal{G}^{(i)}$ is more affected by losses. More on this topic will be discussed later.

Finally, for the scenario with $\pm\varphi/2$ internal phase shifts and external phase reference available the QFI $\mathcal{F}^{(ii)}$ (thin solid green curve) maximizes in the balanced case too. Its lossy counterpart $\mathcal{G}^{(ii)}$ (thick dotted light-green curve for $\eta_2 = 0.9$) at first, similarly to the other two QFI scenarios, seems to drift its maximum towards $T = 1$ (dashed-dotted green curve). However, as losses increase, the optimum $T^{(ii)}_{\text{opt}}$ drifts back towards the balanced case eventually arriving at $T^{(ii)}_{\text{opt}} = 0$ for $\eta_2 = 0$, yielding $\mathcal{G}^{(ii)}(0) \approx |\alpha|^2$ as required by Eq. (39).

In Fig. 5 (upper subfigure) we depict the three balanced penalties versus the loss rate coefficient $1 - \eta_2$. As expected, in the lossless case, the QFI for each scenario shows no or very small balanced penalties. However, as losses increase, both $\mathcal{P}^{(2p)}$ (solid blue curve) and especially $\mathcal{P}^{(i)}$ (dotted red curve) increase, reaching both the maximum value of $\sqrt{2}$ for

[1]By applying the high-coherent approximation to Eq. (C6) from [40], one gets the result

$$\mathcal{G}^{(i)} \approx \frac{2\eta_2|\alpha|^2\cosh r}{\cosh r - \eta_2 \sinh r}.$$

$\eta_2 \to 0$. In the lower subfigure, the corresponding optimum BS_1 transmission coefficients are depicted. Finally, $\mathcal{P}^{(ii)}$ (dashed-dotted green curve) shows a more complex behavior. As losses increase, it first increases, too, with a maximum reached around $1-\eta_2 = 0.4$. It then decreases back to $\mathcal{P}^{(ii)} = 1$ for $1-\eta_2 \approx 0.9$ only to increase again as $1-\eta_2 \to 1$. Its corresponding optimum BS_1 transmission coefficient is plotted in the lower subfigure (dotted thick green curve).

C. Coherent plus Fock input state

We now consider the coherent plus Fock input state [61–63]

$$|\psi_{\text{in}}\rangle = |\alpha_1 n_0\rangle, \tag{100}$$

where $|n_0\rangle$ denotes a Fock state in input port 0, i.e., $\hat{n}_0|n_0\rangle = n|n_0\rangle$. The two-parameter QFI in the lossless limit $\eta_2 \to 1$ was already reported in the literature [32],

$$\mathcal{F}^{(2p)} = \sin^2\vartheta\,[|\alpha|^2 + n(2|\alpha|^2+1)], \tag{101}$$

and it maximizes in the balanced case to [62,63]

$$\mathcal{F}^{(2p)}_{\text{max}} = |\alpha|^2 + n(2|\alpha|^2+1). \tag{102}$$

From Eq. (6) we find

$$\langle \hat{n}_3\rangle = |\alpha|^2\cos^2\frac{\vartheta}{2} + n\,\sin^2\frac{\vartheta}{2} \tag{103}$$

and the two-parameter lossy QFI $\mathcal{G}^{(2p)}$ is given in Eq. (K1). The optimum $T^{(2p)}_{\text{opt}}$ maximizing the QFI $\mathcal{G}^{(2p)}$ is given in Appendix K. In the experimentally interesting high-coherent regime (i.e., $|\alpha| \gg n$) we can approximate the previous QFI to

$$\mathcal{G}^{(2p)} \approx \frac{2\eta_2|\alpha|^2(1+2n)\sin^2\vartheta\,(1+\cos\vartheta\,)}{(1-\eta_2)(1+2n)\sin^2\vartheta + 2\eta_2(1+\cos\vartheta\,)}, \tag{104}$$

and the optimum BS_1 transmission coefficient maximizing is found to be

$$T^{(2p)}_{\text{opt}} \approx \sqrt{1+\sqrt{\eta_2}\,\frac{\sqrt{\frac{\eta_2}{1+2n}} - \sqrt{1-\frac{2\eta_2 n}{1+2n}}}{(1-\eta_2)\sqrt{1+2n}}}. \tag{105}$$

Setting $n=0$ in the previous equation (i.e., we have a single coherent input) allows us to recover the result from Eq. (50).

For the asymmetric single-parameter QFI, in the lossless case we have [32]

$$\mathcal{F}^{(i)} = \sin^2\vartheta\,(2|\alpha|^2+1)n + 4|\alpha|^2\cos\frac{\vartheta}{2} \tag{106}$$

and, similar to the previous input states, via Eqs. (36) and (103) one obtains its lossy counterpart $\mathcal{G}^{(i)}$. If we assume once again the $|\alpha|^2 \gg n$ regime, the previous equation can be approximated to

$$\mathcal{G}^{(i)} \approx \frac{4\eta_2|\alpha|^2\cos^2\frac{\vartheta}{2}\left(2\,\sin^2\frac{\vartheta}{2}n+1\right)}{(1-\eta_2)\left(2\,\sin^2\frac{\vartheta}{2}n+1\right)+\eta_2} \tag{107}$$

leading to the optimum BS_1 transmission coefficient

$$T^{(i)}_{\text{opt}} \approx \sqrt{1+\frac{1-\sqrt{\eta_2[1+2n(1-\eta_2)]}}{2n(1-\eta_2)}}, \tag{108}$$

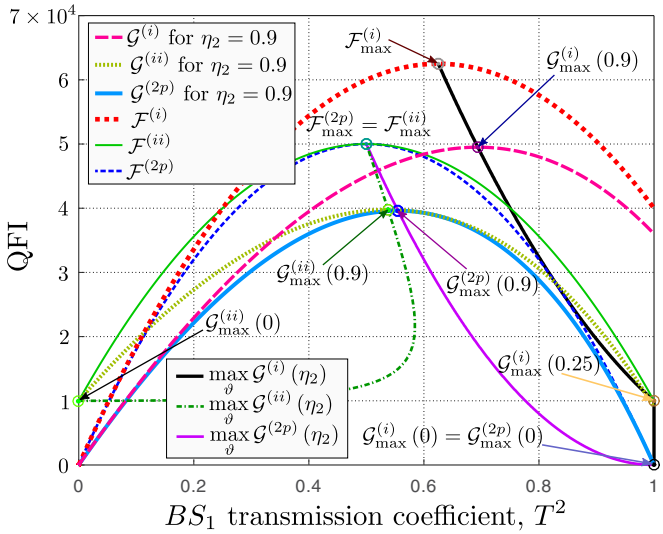

FIG. 6. The lossy QFI in the three considered scenarios for a coherent plus Fock input state. Each circle marks the maximum of the corresponding curve. The maxima $\mathcal{G}^{(i)}_{\text{max}}(\eta_2)$, $\mathcal{G}^{(2p)}_{\text{max}}(\eta_2)$, and, respectively, $\mathcal{G}^{(ii)}_{\text{max}}(\eta_2)$ as η_2 is varied from 1 to 0 are depicted via the solid black, the dashed-dotted green, and, respectively, the solid magenta curves. Parameters used: $|\alpha| = 10^2$, $n = 2$.

and the previous expression (being the result of an approximation) is meaningful as long as $T^{(i)}_{\text{opt}} \leqslant 1$.

Finally, the symmetric single-parameter QFI in the lossless scenario is [32]

$$\mathcal{F}^{(ii)} = \sin^2\vartheta\,(2|\alpha|^2+1)n + |\alpha|^2 \tag{109}$$

and it maximizes to $\mathcal{F}^{(ii)} = |\alpha|^2(2n+1)+n$ [72] in the balanced case. Its lossy counterpart $\mathcal{G}^{(ii)}$ is obtained from Eq. (40). Contrary to the other two QFI scenarios, as $\eta_2 \to 0$ we arrive at a non-null QFI value and it maximizes for $T^{(ii)}_{\text{opt}} \to 0$, yielding

$$\mathcal{G}^{(ii)}_{\text{max}}(0) = |\alpha|^2. \tag{110}$$

In the high-coherent input approximation, one can easily find the optimum BS_1 transmission coefficient maximizing $\mathcal{G}^{(ii)}$ [see Eq. (K4) from Appendix K] and we get

$$T^{(ii)}_{\text{opt}} \approx \sqrt{1+\frac{2\sqrt{\eta_2}-(1+\eta_2)\sqrt{1+2n(1-\eta_2)}}{4(1-\eta_2)\sqrt{\eta_2}n}} \tag{111}$$

valid for $n \neq 0$ and this $T^{(ii)}_{\text{opt}}$ leads to the maximum symmetric single-parameter QFI given in Eq. (K5).

In Fig. 6 we depict the corresponding QFI in all three discussed scenarios versus the transmission coefficient of BS_1. The two-parameter lossless QFI, $\mathcal{F}^{(2p)}$ (dashed blue curve), as discussed in the literature [32], reaches its maximum in the balanced case. For the chosen loss coefficient ($\eta_2 = 0.9$) its lossy counterpart $\mathcal{G}^{(2p)}$ (solid light-blue curve) maximizes for values $T^{(2p)}_{\text{opt}} > \sqrt{0.5}$ as easily verified from Eq. (105). This optimum slowly drifts towards 1 as losses increase, and for $\eta_2 = 0$ we have $T^{(2p)}_{\text{opt}} = 1$. The evolution of the maxima $\mathcal{G}^{(2p)}_{\text{max}}(\eta_2)$ as η_2 goes from 1 to 0 (thin solid magenta curve) is also depicted in Fig. 6.

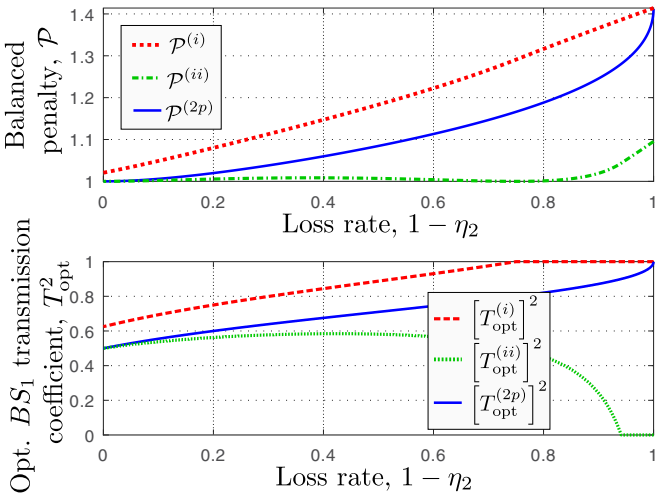

FIG. 7. The balanced penalties in the three considered scenarios for a coherent plus Fock input state versus the loss rate $1-\eta_2$ (upper subfigure) and the corresponding optimum transmission coefficients (lower subfigure). Parameters used: $|\alpha| = 10^2$, $n = 2$.

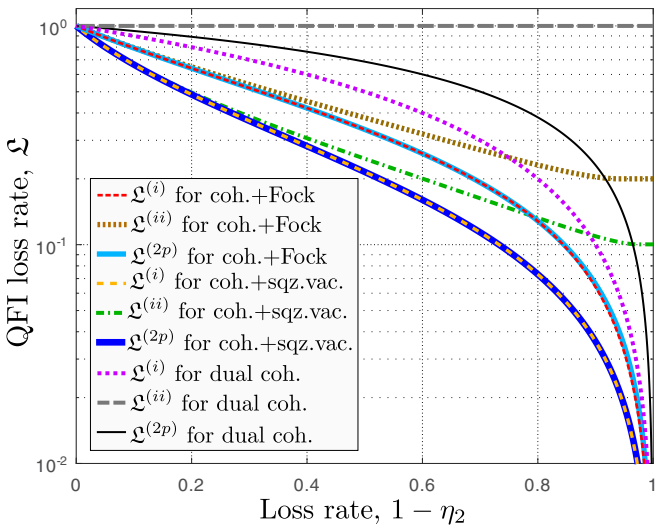

FIG. 8. The QFI loss rates $\mathfrak{L}^{(i)}$, $\mathfrak{L}^{(ii)}$, and $\mathfrak{L}^{(2p)}$ versus the loss rate $1-\eta_2$ for three input states (see main text for details), all featuring a coherent state in port 1. Parameters used: $|\alpha| = 10^2$, while in input port 0 we have $\langle \hat{n}_0 \rangle \approx 2$ for all three states.

The asymmetric single-parameter QFI $\mathcal{F}^{(i)}$ (thick dotted red curve) maximizes in the unbalanced case ($T^{(i)}_{\rm opt} \approx \sqrt{0.66}$ for our parameters). Its lossy counterpart $\mathcal{G}^{(i)}$ (dashed pink curve for $\eta_2 = 0.9$) continues this trend ($T^{(i)}_{\rm opt} \approx \sqrt{0.69}$ for $\eta_2 = 0.9$) until in reaches $T^{(i)}_{\rm opt} = 1$ for $\eta_{2\rm lim} = 0.25$ as given by Eq. (63). The maxima $\mathcal{G}^{(i)}_{\rm max}(\eta_2)$ for each value η_2 from 1 down to 0 are also depicted (solid black curve).

Finally, $\mathcal{F}^{(ii)}$ (thin solid green curve) maximizes in the balanced case, too. In the lossy scenario $\mathcal{G}^{(ii)}$ (thick dotted light-green curve for $\eta_2 = 0.9$), as expected, no longer maximizes in the balanced case. Indeed, similar to the coherent plus squeezed vacuum from Fig. 4, $\mathcal{G}^{(ii)}_{\rm max}(\eta_2)$ (dashed-dotted green curve) first drifts beyond $T^2 = 0.5$ and, as losses increase, the optimum $T^{(ii)}_{\rm opt}$ drifts back arriving at $T^{(ii)}_{\rm opt} = 0$ for $\eta_2 = 0$ yielding for $\mathcal{G}^{(ii)}(0)$ the value given by Eq. (39).

In Fig. 7 we plot the balanced penalties in the three considered scenarios for a coherent plus Fock input state. While both $\mathcal{P}^{(ii)}$ and $\mathcal{P}^{(2p)}$ start at a value of 1 (i.e., no penalty) in the lossless case, for $\mathcal{P}^{(i)}$ we have $\mathcal{P}^{(i)}(1) = 0.9$. As the losses increase both $\mathcal{P}^{(2p)}$ and $\mathcal{P}^{(i)}$ rapidly rise, reaching the value $\sqrt{2}$ for $\eta_2 \to 0$. The balanced penalty $\mathcal{P}^{(ii)}$ has a more complex behavior, however, it stays close to 1, this scenario thus not benefiting much in the unbalanced case.

Finally, after having discussed the double coherent (Sec. VI A), the coherent plus squeezed vacuum (Sec. VI B), and the coherent plus Fock input states, we can compare their immunity to losses via the QFI loss rates defined in Sec. V A. In Fig. 8 we plot the QFI loss rates (i.e., $\mathfrak{L}^{(i)}$, $\mathfrak{L}^{(ii)}$, and $\mathfrak{L}^{(2p)}$) versus the loss rate $1-\eta_2$ for the three aforementioned input states. In order to have a fair comparison, for all considered inputs we apply a coherent state ($|\alpha| = 10^2$) in port 1 and the same average number of photons $\langle \hat{n}_0 \rangle \approx 2$ in input port 0. More precisely, we considered $|\beta| = \sqrt{2}$ for the double coherent, $r = 1.15$ for the coherent plus squeezed vacuum, and $n = 2$ for coherent plus Fock input states. When applicable, we also imposed the optimum input PMC.

As a general rule, for each input state, the most immune to losses proves to be $\mathfrak{L}^{(ii)}$, its limit value as $\eta_2 \to 0$ reaching a plateau, i.e., $\mathfrak{L}^{(ii)}(0) \neq 0$ [see Eq. (39)]. The next resilience to losses is found for $\mathfrak{L}^{(2p)}$ and the least one will prove to be $\mathfrak{L}^{(i)}$. This phenomenon can be explained by the fact that in the scenario not having access to an external phase reference, the lossless case is almost always balanced. Hence, part of the losses are compensated by unbalancing the interferometer.

Ranking now the resilience of the different input states considered, the double coherent input defined by Eq. (74) proves to be the most resilient state when it comes to losses, with the QFI $\mathcal{G}^{(ii)}$ being totally immune to them, as seen from Eq. (85). This performance can be explained by the fact that this state is both unentangled after BS_1 and also does not surpass the SNL for the lossless case (hence, there is not much "quantum advantage" to be lost). The next best resistance to losses is shown by the coherent plus Fock input state for the symmetric single-parameter QFI [we find $\mathfrak{L}^{(ii)}(0) \approx 1/(2n+1) = 0.2$] followed by the same QFI scenario with a coherent plus squeezed vacuum input [$\mathfrak{L}^{(ii)}(0) = e^{-2r} \approx 0.1$].

D. Double Fock input state

The double Fock [64,73] input is a well-known profoundly nonclassical and non-Gaussian state

$$|\psi_{\rm in}\rangle = \frac{(\hat{a}_0^\dagger)^m}{\sqrt{m!}} \frac{(\hat{a}_1^\dagger)^n}{\sqrt{n!}} |0_0 0_1\rangle = |m_0 n_1\rangle. \tag{112}$$

Quite remarkably, in the lossless case, for this input state all three considered scenarios yield exactly the same QFI, namely [32],

$$\mathcal{F} = \mathcal{F}^{(i)} = \mathcal{F}^{(ii)} = \mathcal{F}^{(2p)} = \sin^2 \vartheta (2mn + m + n) \tag{113}$$

and they are obviously maximized in the balanced case, yielding

$$\mathcal{F}_{\rm max} = \mathcal{F}^{(i)}_{\rm max} = \mathcal{F}^{(ii)}_{\rm max} = \mathcal{F}^{(2p)}_{\rm max} = 2mn + m + n. \tag{114}$$

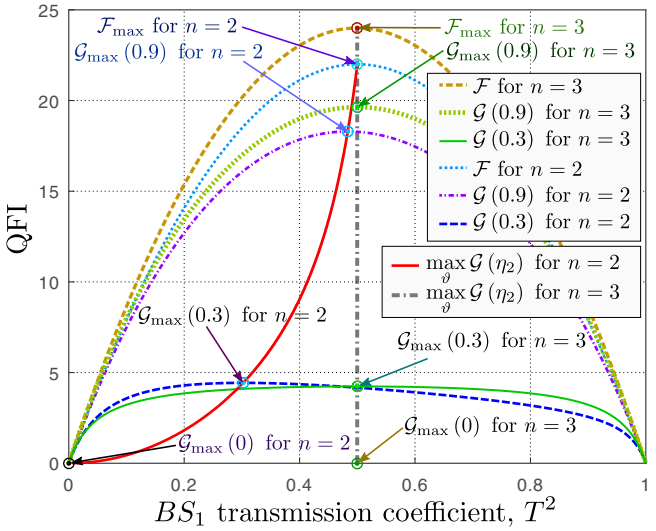

FIG. 9. The QFI for a double Fock input state and a fixed number total number of photons $\langle\hat{N}\rangle = 6$. Two scenarios are depicted: $n = 3$ (i.e., $m = 3$) and $n = 2$ (i.e., $m = 4$).

Equally remarkably, in the lossy case we get

$$\mathcal{G} = \mathcal{G}^{(i)} = \mathcal{G}^{(ii)} = \mathcal{G}^{(2p)} = \frac{\eta_2 \sin^2\vartheta[m+n-(m-n)\cos\vartheta]}{\frac{(1-\eta_2)\sin^2\vartheta}{2} + \frac{\eta_2[m+n-(m-n)\cos\vartheta]}{2mn+m+n}} \tag{115}$$

and this time the maximization does not necessarily happen in the balanced case (see Appendix L). For the special case $m = n$, i.e., we have a twin-Fock input $|\psi_{\text{in}}\rangle = |n_1 n_0\rangle$, Eq. (115) becomes

$$\mathcal{G} = \frac{4\eta_2 n(n+1)\sin^2\vartheta}{(1-\eta_2)(n+1)\sin^2\vartheta + 2\eta_2}, \tag{116}$$

and balancing BS_1 ($\vartheta_{\text{opt}} = \pi/2$) leads to the maximum lossy QFI

$$\mathcal{G}_{\max} = \frac{4\eta_2 n(n+1)}{n(1-\eta_2)+1+\eta_2}. \tag{117}$$

We thus have the QFI loss rate(s)

$$\mathfrak{L} = \frac{2\eta_2}{n(1-\eta_2)+1+\eta_2}. \tag{118}$$

It can be easily shown that given the constraint of a fixed total number of input photons $\langle\hat{N}\rangle$, the lossless QFI $\mathcal{F}$ maximizes for $n = m$. This, however, as we will see shortly, is not true any more in the lossy case.

In Fig. 9 we plot the lossy QFI $\mathcal{G}$ in respect with the transmission coefficient of BS_1 for a fixed number of input photons $\langle\hat{N}\rangle = 6$ and two cases, namely, $n = m = 3$ and $m = 4$ ($n = 2$). In the lossless case the $n = m$ case outperforms the other one, as expected. The same remains true for low losses (i.e., $\eta_2 = 0.9$). However, for higher losses ($\eta_2 = 0.3$), this is no longer true.

Moreover, for the case $n = m = 3$, as previously remarked, the QFI maximizes in the balanced case. This is no longer true for $m \neq n$. In Fig. 9 we plot $\mathcal{G}_{\max}(\eta_2)$ as function of η_2 (solid red curve) for $m = 4$ and $n = 2$ as well as for $m = n = 3$ (vertical dashed-dotted dark gray line).

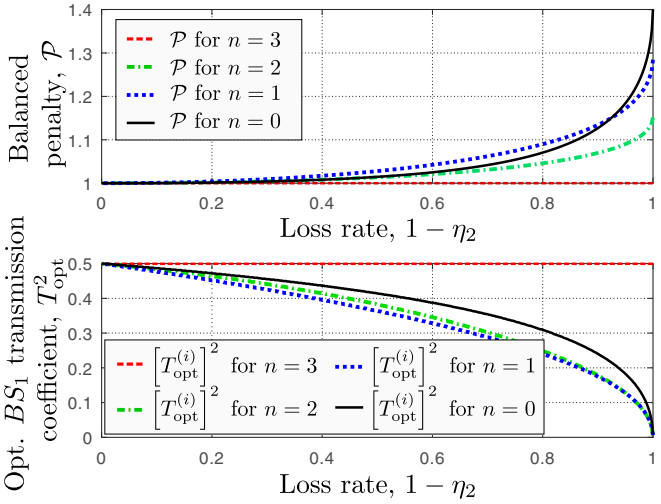

FIG. 10. The balanced penalties and the corresponding optimum transmission coefficient for a dual Fock input state with constraint total number of input photons $\langle\hat{N}\rangle = 6$ and four scenarios. Details are given in the main text.

In Fig. 10 we plot the balanced penalty $\mathcal{P}$ for $\langle\hat{N}\rangle = 6$ and four scenarios ($n = 0$, 1, 2, and 3). Except the scenario $n = m$, the balanced penalty increases with the loss rate. At high losses, the maximum $\mathcal{P} = \sqrt{2}$ is reached for $n = 0$. The corresponding optimum transmission coefficients T_{opt} are plotted in the lower subfigure.

One can ask the following question: for a fixed total number of input photons $\langle\hat{N}\rangle = m + n$, how should one distribute them in a double Fock input so that the lossy QFI $\mathcal{G}$ is maximized? As depicted in Fig. 11 (upper subfigure), the answer depends on the loss coefficient. For very low losses, as expected from the lossless case, the distribution $n = m$ yields the highest QFI. As losses increase, though, a more and

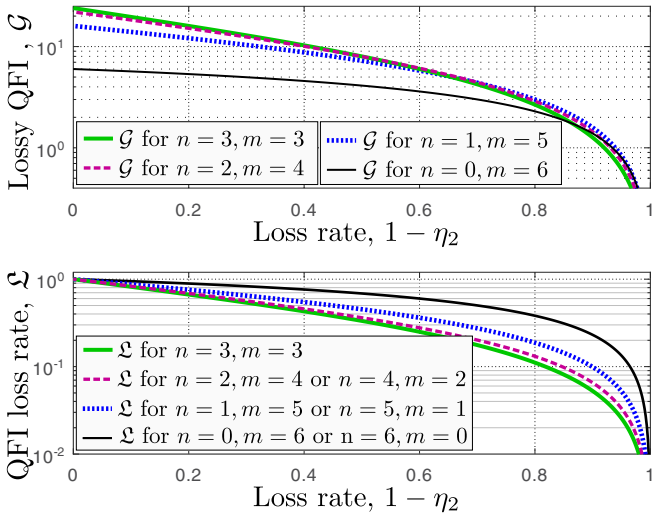

FIG. 11. The lossy QFI $\mathcal{G}$ (upper subfigure) and the QFI loss rate $\mathfrak{L}$ (lower subfigure) for a double Fock input state versus the loss rate $1-\eta_2$. We imposed the constraint of a fixed total number of input photons and varied the individual photons in one input port. See main text for details. Parameter used: $\langle\hat{N}\rangle = 6$.

more uneven distribution of the photons between the two input ports yields the maximal QFI, culminating, in the high-loss regime $\eta_2 \ll 1-\eta_2$, with $m = \langle\hat{N}\rangle$ and $n = 0$ (or $m = 0$ and $n = \langle\hat{N}\rangle$).

One can also ask the same question relative to the resilience to losses. We answer this question in Fig. 11 (lower subfigure). It turns out that the worst resilience to losses for a double Fock input state is found for $n = m$ and $\mathfrak{L}$ is given by Eq. (118). The best resilience to losses happens either when $m = \langle\hat{N}\rangle$ and $n = 0$ or when $n = \langle\hat{N}\rangle$ and $m = 0$ and the QFI loss rate is given this time by Eq. (53).

E. Two-mode squeezed vacuum input state

Finally, let us consider the two-mode squeezed vacuum (TMSV) [41,52] input state

$$|\psi_{\text{in}}\rangle = \hat{S}_{\text{tm}}(\xi)|0_0 0_1\rangle, \tag{119}$$

where the two-mode squeezing operator is defined by [52]

$$\hat{S}_{\text{tm}}(\xi) = e^{\xi^* \hat{a}_0 \hat{a}_1 - \xi \hat{a}_0^\dagger \hat{a}_1^\dagger} \tag{120}$$

and we have the input average number of photons $\langle\hat{N}\rangle = 2\sinh^2 r$. The QFI for all considered scenarios in the lossless case have already been reported in the literature [32,41]. The two-parameter and the symmetric single-parameter QFI yield the same value,

$$\mathcal{F}^{(ii)} = \mathcal{F}^{(2p)} = \sin^2\vartheta\ \sinh^2 2r, \tag{121}$$

and they both maximize in the balanced case yielding

$$\mathcal{F}^{(ii)}_{\text{max}} = \mathcal{F}^{(2p)}_{\text{max}} = \sinh^2 2r = 4\langle\hat{N}\rangle(\langle\hat{N}\rangle + 2). \tag{122}$$

For the lossy two-parameter QFI one gets

$$\mathcal{G}^{(2p)} = \frac{\eta_2 \sinh^2 2r\ \sin^2\vartheta}{\eta_2 + (1-\eta_2)\cosh^2 r\ \sin^2\vartheta} \tag{123}$$

and this QFI maximizes in the balanced case yielding

$$\mathcal{G}^{(2p)}_{\text{max}} = \frac{\eta_2 \sinh^2 2r}{\eta_2 + (1-\eta_2)\cosh^2 r}, \tag{124}$$

a result also reported in Ref. [44].

For the asymmetric single-parameter QFI we have

$$\mathcal{F}^{(i)} = (1+\sin^2\vartheta)\sinh^2 2r \tag{125}$$

and this value is maximized in the balanced case yielding $\mathcal{F}^{(i)}_{\text{max}} = 2\sinh^2 2r$ [32]. We also remark the simple relation $\mathcal{F}^{(i)}_{\text{max}} = 2\mathcal{F}^{(2p)}_{\text{max}}$. In the lossy case, the asymmetric single-parameter QFI from Eq. (35) gives

$$\mathcal{G}^{(i)} = \frac{\eta_2 \sinh^2 2r(1+\sin^2\vartheta)}{(1-\eta_2)\cosh^2 r(1+\sin^2\vartheta)+\eta_2} \tag{126}$$

which maximizes in the balanced case yielding (result also reported in Ref. [40])

$$\mathcal{G}^{(i)}_{\text{max}} = \frac{2\eta_2 \sinh^2 2r}{\eta_2 + (1-\eta_2)\cosh^2 r}, \tag{127}$$

and similar to the lossless case we have the relation $\mathcal{G}^{(i)}_{\text{max}} = 2\mathcal{G}^{(2p)}_{\text{max}}$. We thus have the QFI loss rates

$$\mathfrak{L}^{(i)} = \mathfrak{L}^{(2p)} = \frac{\eta_2}{\eta_2 + (1-\eta_2)\cosh^2 r}. \tag{128}$$

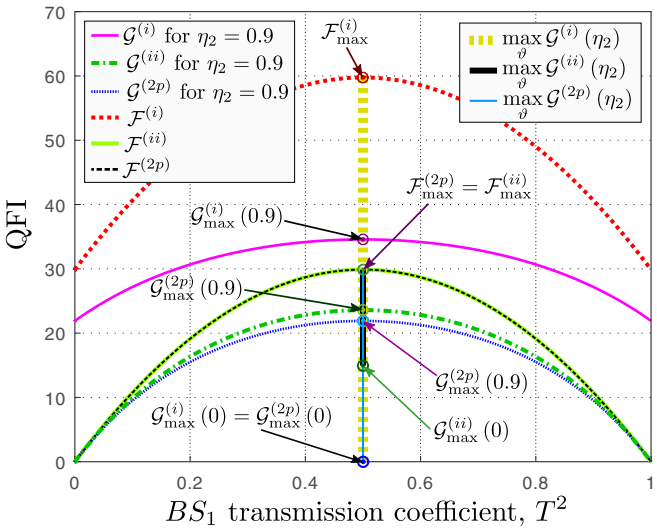

FIG. 12. The QFI in the three lossy scenarios for a TMSV input state. Regardless of the scenario and of the loss coefficient η_2, each time the QFI maximizes in the balanced case. Parameter used: $r = 1.2$.

In the high-loss regime, as expected, both $\mathcal{G}^{(2p)}$ and $\mathcal{G}^{(i)}$ tend to zero leading to $\mathfrak{L}^{(i)}(0) = \mathfrak{L}^{(2p)}(0) = 0$.

Finally, for the symmetric single-parameter QFI we have in the lossless case $\mathcal{F}^{(ii)} = \sinh^2 2r\ \sin^2\vartheta$ [32] maximizing for $\vartheta = \pi/2$ to $\mathcal{F}^{(ii)}_{\text{max}} = \sinh^2 2r$ while in the lossy scenario we have

$$\mathcal{G}^{(ii)} = \frac{\sinh^2 2r\ \sin^2\vartheta(\cosh^2 r - \eta_2 \sinh^2 r)}{(1-\eta_2)\cosh^2 r(1+\sin^2\vartheta)+\eta_2} \tag{129}$$

and it is maximized, too, in the balanced case leading to

$$\mathcal{G}^{(ii)}_{\text{max}} = \frac{\sinh^2 2r(\cosh^2 r - \eta_2 \sinh^2 r)}{2(1-\eta_2)\cosh^2 r + \eta_2}. \tag{130}$$

The QFI loss rate is

$$\mathfrak{L}^{(ii)} = \frac{\cosh^2 r - \eta_2 \sinh^2 r}{2(1-\eta_2)\cosh^2 r + \eta_2}, \tag{131}$$

and as $\eta_2 \to 0$ we have

$$\mathcal{G}^{(ii)}(0) = \frac{\sinh^2 2r}{2}, \tag{132}$$

leading to the maximum QFI loss rate

$$\mathfrak{L}^{(ii)}(0) = 0.5. \tag{133}$$

In Fig. 12 we depict the three considered QFI scenarios in respect with the transmission coefficient of BS_1. As discussed previously, all maximize in the balanced case. Both $\mathcal{G}^{(i)}$ and $\mathcal{G}^{(2p)}$ show very low resilience to losses, and for high losses, from Eq. (128) we have the scaling

$$\mathfrak{L}^{(i)} = \mathfrak{L}^{(2p)} \approx \frac{\eta_2}{(1-\eta_2)\cosh^2 r}. \tag{134}$$

Thus, the higher the squeezing factor, the more impacted the QFI loss rate is. However, for the symmetric single-parameter QFI, as seen from Fig. 12, the impact of losses is very limited, even as $\eta_2 \to 0$, as proven also by Eq, (133).

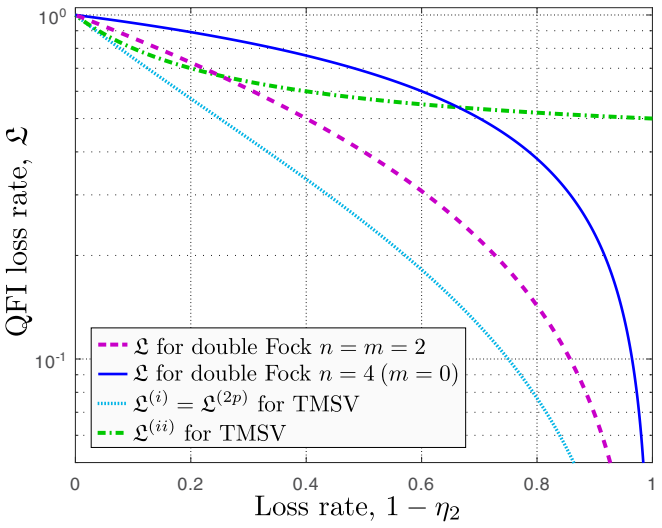

FIG. 13. The QFI loss rate $\mathfrak{L}$ for the double Fock and TMSV input states versus the loss rate $1-\eta_2$. For a small loss coefficient the double Fock (solid blue curve) outperforms all other scenarios. However, the most resilient to losses is $\mathfrak{L}^{(ii)}$ for a TMSV input. Parameters used: $\langle\hat{N}\rangle=4$ and $r=1.15$.

Since the QFI maximizes in the balanced case in all scenarios, we have unit balanced penalties, i.e.,

$$\mathcal{P}^{(2p)}(\eta_2)=\mathcal{P}^{(i)}(\eta_2)=\mathcal{P}^{(ii)}(\eta_2)=1. \tag{135}$$

In Fig. 13 we compare the double Fock and TMSV input states in terms of QFI loss rates. The TMSV input state is outperformed by any combination of double Fock input when it comes to $\mathfrak{L}^{(i)}$ and $\mathfrak{L}^{(2p)}$. The same is true for $\mathfrak{L}^{(ii)}$ for low losses. However, as losses increase, contrary to any combination of double Fock input (where $\mathfrak{L}^{(ii)}\to 0$), the QFI loss rate $\mathfrak{L}^{(ii)}$ for a TMSV input saturates at 0.5.

VII. CONCLUSIONS

In this paper we addressed the problem of quantum Fisher information maximization in an unbalanced, lossy interferometer. We considered three scenarios and provided closed-form expressions for the QFI with a generic input for all of them.

We introduced a metric called balanced penalty, able to quantify the loss in terms of optimal phase sensitivity for a balanced interferometer in respect with an optimized, unbalanced one. We also introduced the QFI loss rate as a metric to quantify the immunity of a given scheme and input state to losses.

We also addressed the problem of QFI maximization via the optimization of the transmission coefficient of the first beam splitter. We discussed both the single- and two-parameter QFI and were able to give closed-form results for a number of scenarios. These results were applied to a number of Gaussian and non-Gaussian input states, discussing at length their respective QFI maximization.

We conclude that in the lossy scenario, the maximum QFI is obtained almost always in the unbalanced case. This conclusion applies to both the single- and two-parameter QFI scenarios.

ACKNOWLEDGMENT

The Authors acknowledge the support of contract PN 23 21 01 05 funded by the Romanian Ministry of Research, Innovation and Digitalization and of the Extreme Light Infrastructure Nuclear Physics Phase II, a project co-financed by the Romanian Government and the European Union through the European Regional Development Fund and the Competitiveness Operational Programme (No. 1/07.07.2016, COP, ID 1334).

APPENDIX A: BS_1 INPUT-OUTPUT PHOTON-NUMBER VARIANCES AND COVARIANCES TRANSFORMATIONS

The variance of the operators $\hat{n}_2$ and $\hat{n}_3$ as well as their covariance in respect with the input fields are

$$\begin{cases}\Delta^2\hat{n}_2=\dfrac{\Delta^2\hat{N}}{4}+\sin^2\vartheta\,\Delta^2\hat{J}_y+\cos^2\vartheta\,\Delta^2\hat{J}_z-\sin 2\vartheta\,\widehat{\mathrm{Cov}}(\hat{J}_y,\hat{J}_z)-\sin\vartheta\,\mathrm{Cov}(\hat{J}_y,\hat{N})+\cos\vartheta\,\mathrm{Cov}(\hat{J}_z,\hat{N}),\\ \Delta^2\hat{n}_3=\dfrac{\Delta^2\hat{N}}{4}+\sin^2\vartheta\,\Delta^2\hat{J}_y+\cos^2\vartheta\,\Delta^2\hat{J}_z-\sin 2\vartheta\,\widehat{\mathrm{Cov}}(\hat{J}_y,\hat{J}_z)+\sin\vartheta\,\mathrm{Cov}(\hat{N},\hat{J}_y)-\cos\vartheta\,\mathrm{Cov}(\hat{N},\hat{J}_z),\\ \mathrm{Cov}(\hat{n}_2,\hat{n}_3)=\dfrac{\Delta^2\hat{N}}{4}-\sin^2\vartheta\,\Delta^2\hat{J}_y-\cos^2\vartheta\,\Delta^2\hat{J}_z+\sin 2\vartheta\,\widehat{\mathrm{Cov}}(\hat{J}_y,\hat{J}_z).\end{cases} \tag{A1}$$

APPENDIX B: THE C COEFFICIENTS FOR THE TWO-PARAMETER QFI

The C coefficients from Sec. III are defined by [32]

$$\begin{cases}C_0=4\left(\Delta^2\hat{J}_z-\dfrac{[\mathrm{Cov}(\hat{J}_z,\hat{N})]^2}{\Delta^2\hat{N}}\right),\\ C_1=16\left(\Delta^2\hat{J}_y-\Delta^2\hat{J}_z-\dfrac{[\mathrm{Cov}(\hat{J}_y,\hat{N})]^2}{\Delta^2\hat{N}}+\dfrac{[\mathrm{Cov}(\hat{J}_z,\hat{N})]^2}{\Delta^2\hat{N}}\right),\\ C_2=-16\left(\widehat{\mathrm{Cov}}(\hat{J}_y,\hat{J}_z)-\dfrac{\mathrm{Cov}(\hat{J}_y,\hat{N})\mathrm{Cov}(\hat{J}_z,\hat{N})}{\Delta^2\hat{N}}\right).\end{cases} \tag{B1}$$

If $\Delta^2\hat{N}=0$, the above coefficients are replaced with the ones given by Eq. (22).

APPENDIX C: THE C' COEFFICIENTS FOR THE SINGLE-PARAMETER QFI

The result from [32], i.e., $\mathcal{F}^{(i)} = C'_0 + |TR|^2 C'_1 + |TR|(|T|^2 - |R|^2)C'_2 + (|T|^2 - |R|^2)C'_3 + |TR|C'_4$ can be recast in a ϑ formulation via the equivalences $|T|^2 - |R|^2 = \cos\vartheta$ and $|TR| = \frac{\sin\vartheta}{2}$ yielding the result stated by Eq. (20). The C' coefficients are given by

$$\begin{cases} C'_0 = 4\Delta^2\hat{J}_z + \Delta^2\hat{N}, \\ C'_1 = 16(\Delta^2\hat{J}_y - \Delta^2\hat{J}_z), \\ C'_2 = -16\,\widehat{\mathrm{Cov}}(\hat{J}_y, \hat{J}_z), \\ C'_3 = -4\,\mathrm{Cov}(\hat{J}_z, \hat{N}), \\ C'_4 = 8\,\mathrm{Cov}(\hat{J}_y, \hat{N}). \end{cases} \tag{C1}$$

APPENDIX D: QFI FORMALISM FOR THE LOSSY CASE

In the formalism modeling a lossy interferometer we mainly follow [50], adapting it to two internal phase shifts (see also [55,74]). The total wave vector of the system is extended to include the environment. As discussed in Sec. II, we model the losses via fictitious beam splitters in the upper (lower) arm and having a transmission coefficient $\sqrt{\eta_1}$ ($\sqrt{\eta_2}$). The input of these beam spitters is always the vacuum state, i.e., $|0_{\boldsymbol{v}}\rangle = |0_{v2}0_{v3}\rangle$. The total system (interferometer + environment) follows a unitary evolution $\hat{U}_{\mathrm{IE}}(\varphi_1, \varphi_2)$ resulting in the global wave vector (see Fig. 1),

$$|\Psi_t\rangle = \hat{U}_{\mathrm{IE}}(\varphi_1, \varphi_2)|\psi_{23}\rangle\big|0_{v_2}0_{v_3}\big\rangle = \sum_{m,m'} \hat{\Pi}_{m,m'}(\varphi_1, \varphi_2)|\psi\rangle\big|m_{o_2}m'_{o_3}\big\rangle, \tag{D1}$$

where $|m_{o2}\rangle$ ($|m'_{o_3}\rangle$) models m (m') photons lost in the upper (lower) arm. The Kraus operators are

$$\hat{\Pi}_{m,m'}(\varphi_1, \varphi_2) = \big\langle m_{o_2}m'_{o_3}\big|\hat{U}_{\mathrm{IE}}(\varphi_1, \varphi_2)\big|0_{v_2}0_{v_3}\big\rangle. \tag{D2}$$

Similar to the lossless case, we can perform the variable change from Eq. (8) and reexpress both Eqs. (D1) and (D2) in respect with the sum and difference phases φ_s and φ_s. We end up with a 2×2 Fisher matrix

$$\boldsymbol{C} = \begin{pmatrix} \mathcal{C}_{ss} & \mathcal{C}_{sd} \\ \mathcal{C}_{sd} & \mathcal{C}_{dd} \end{pmatrix}. \tag{D3}$$

The elements $\mathcal{C}_{kl}$ ($k, l \in \{s, d\}$) can be obtained in the usual manner for pure states (see [50,74]) and we have

$$\mathcal{C}_{kl} = 4\left(\left\langle\frac{\partial\Psi_t}{\partial\varphi_k}\middle|\frac{\partial\Psi_t}{\partial\varphi_l}\right\rangle^2 - \left\langle\frac{\partial\Psi_t}{\partial\varphi_k}\middle|\Psi_t\right\rangle\left\langle\Psi_t\middle|\frac{\partial\Psi_t}{\partial\varphi_l}\right\rangle\right) = 4\big(\langle\hat{H}_{k,l}\rangle - \langle\hat{h}^{(k)}_{k,l}\rangle\langle\hat{h}^{(l)}_{k,l}\rangle\big), \tag{D4}$$

where we denoted

$$\begin{aligned} \hat{H}_{k,l} &= \sum_{m,m'} \frac{d\hat{\Pi}^\dagger_{m,m'}}{\partial\varphi_k}\frac{d\hat{\Pi}_{m,m'}}{\partial\varphi_l}, \\ \hat{h}^{(k)}_{k,l} &= i\sum_{m,m'} \frac{d\hat{\Pi}^\dagger_{m,m'}}{\partial\varphi_k}\hat{\Pi}_{m,m'}, \\ \hat{h}^{(l)}_{k,l} &= -i\sum_{m,m'} \hat{\Pi}^\dagger_{m,m'}\frac{d\hat{\Pi}_{m,m'}}{\partial\varphi_l}. \end{aligned} \tag{D5}$$

For losses in both arms, plausible Kraus operators can be expressed as

$$\hat{\Pi}_{m,m'}(\varphi_s, \varphi_d, \eta_1, \gamma_1, \eta_2, \gamma_2) = \sqrt{\frac{(1-\eta_1)^m}{m!}}\sqrt{\frac{(1-\eta_2)^{m'}}{m'!}}\, e^{i\varphi_d\frac{\hat{n}_2-\hat{n}_3-\gamma_1 m+\gamma_2 m'}{2}} e^{i\varphi_s\frac{\hat{n}_2+\hat{n}_3-\gamma_1 m-\gamma_2 m'}{2}} \eta_1^{\frac{\hat{n}_2}{2}}\eta_2^{\frac{\hat{n}_3}{2}}\hat{a}_2^m\hat{a}_3^{m'}, \tag{D6}$$

where we recall that η_1 (η_2) denotes the loss coefficient in the upper (lower) arm and the position of the photon loss is specified via γ_1 (γ_2) in the upper (lower) arm. For a photon loss before (after) the phase shift we have $\gamma_i = 0$ ($\gamma_i = -1$) for $i = 1, 2$. Since we will employ losses in the lower arm only, we have the simplified Kraus operators

$$\hat{\Pi}_{0,m'}(\varphi_s, \varphi_d, \eta_2, \gamma_2) = \sqrt{\frac{(1-\eta_2)^{m'}}{m'!}}\, e^{i\varphi_d\frac{\hat{n}_2-\hat{n}_3+\gamma_2 m'}{2}} e^{i\varphi_s\frac{\hat{n}_2+\hat{n}_3-\gamma_2 m'}{2}} \eta_2^{\frac{\hat{n}_3}{2}}\hat{a}_3^{m'}. \tag{D7}$$

It is easy to see that in the lossless case ($m' \to 0$ and $\eta_2 \to 1$), the previous equation morphs into the unitary evolution from Eq. (9) and the lossy Fisher matrix elements from (D4) equal the lossless ones from Eq. (10), as expected.

APPENDIX E: LOSSY TWO-PARAMETER QFI

The coefficients of the Fisher matrix elements from Eq. (23) are given by

$$\begin{cases} A_2 = (\gamma_1+1)^2(1-\eta_1)\eta_1, \\ A_3 = (\gamma_2+1)^2(1-\eta_2)\eta_2, \\ V_2 = [1-(\gamma_1+1)(1-\eta_1)]^2, \\ V_3 = [1-(\gamma_2+1)(1-\eta_2)]^2, \\ V_{\rm cov} = 2[1-(\gamma_1+1)(1-\eta_1)][1-(\gamma_2+1)(1-\eta_2)]. \end{cases} \tag{E1}$$

The (nonminimized) lossy two-parameter QFI is found to be

$$\mathcal{C}^{(2p)} = \frac{4(\gamma_2+1)^2(1-\eta_2)\eta_2\Delta^2\hat{n}_2\langle\hat{n}_3\rangle + 4[1-(\gamma_2+1)(1-\eta_2)]^2(\Delta^2\hat{n}_2\Delta^2\hat{n}_3 - [\mathrm{Cov}(\hat{n}_2,\hat{n}_3)]^2)}{\Delta^2\hat{n}_2 + V_3\Delta^2\hat{n}_3 + A_3\langle\hat{n}_3\rangle + V_{\rm cov}\mathrm{Cov}(\hat{n}_2,\hat{n}_3)} \tag{E2}$$

and applying the optimum γ_2 given by Eq. (26) leads to the minimized QFI from Eq. (27). In the case of a nonentangled BS_1 output [i.e., $\mathrm{Cov}(\hat{n}_2,\hat{n}_3)=0$ (see, e.g., [75] for needed conditions] the optimum γ_2 from Eq. (26) simplifies to $\gamma_2^{\rm opt} = \frac{\eta_2 Q_3}{Q_3(1-\eta_2)+1}$ leading to the optimized two-parameter QFI in this scenario

$$\mathcal{G}^{(2p)} = \frac{4\eta_2\langle\hat{n}_3\rangle\Delta^2\hat{n}_2\Delta^2\hat{n}_3}{(1-\eta_2)\Delta^2\hat{n}_2\Delta^2\hat{n}_3 + \eta_2\langle\hat{n}_3\rangle\Delta^2\hat{N}}. \tag{E3}$$

APPENDIX F: MINIMIZED SYMMETRIC SINGLE-PARAMETER QFI IN THE LOSSY CASE WITH LOSSES IN BOTH ARMS

Assuming losses in both arms (see Fig. 2) the symmetric single-parameter lossy QFI is found to be

$$\begin{aligned} \mathcal{C}^{(ii)} = {} & (1-\eta_1)\eta_1(\gamma_1+1)^2\langle\hat{n}_2\rangle + (1-\eta_2)\eta_2(\gamma_2+1)^2\langle\hat{n}_3\rangle + [\eta_1-(1-\eta_1)\gamma_1]^2\Delta^2\hat{n}_2 \\ & + [\eta_2-(1-\eta_2)\gamma_2]^2\Delta^2\hat{n}_3 - 2[\eta_1-(1-\eta_1)\gamma_1][\eta_2-(1-\eta_2)\gamma_2]\mathrm{Cov}(\hat{n}_2,\hat{n}_3) \end{aligned} \tag{F1}$$

result also reported in [45]. This QFI is minimized by imposing

$$\gamma_1^{\rm opt} = -\frac{\eta_1(1-\eta_2)([\mathrm{Cov}(\hat{n}_2,\hat{n}_3)]^2 + \Delta^2\hat{n}_3(\langle\hat{n}_2\rangle - \Delta^2\hat{n}_2)) + \eta_2\langle\hat{n}_3\rangle[\mathrm{Cov}(\hat{n}_2,\hat{n}_3) + \eta_1(\langle\hat{n}_2\rangle - \Delta^2\hat{n}_2)]}{[\eta_1\langle\hat{n}_2\rangle + (1-\eta_1)\Delta^2\hat{n}_2][\eta_2\langle\hat{n}_3\rangle + (1-\eta_2)\Delta^2\hat{n}_3] - (1-\eta_1)(1-\eta_2)[\mathrm{Cov}(\hat{n}_2,\hat{n}_3)]^2} \tag{F2}$$

and

$$\gamma_2^{\rm opt} = -\frac{(1-\eta_1)\eta_2([\mathrm{Cov}(\hat{n}_2,\hat{n}_3)]^2 + \Delta^2\hat{n}_2(\langle\hat{n}_3\rangle - \Delta^2\hat{n}_3)) + \eta_1\langle\hat{n}_2\rangle[\mathrm{Cov}(\hat{n}_2,\hat{n}_3) + \eta_2(\langle\hat{n}_3\rangle - \Delta^2\hat{n}_3)]}{[\eta_1\langle\hat{n}_2\rangle + (1-\eta_1)\Delta^2\hat{n}_2][\eta_2\langle\hat{n}_3\rangle + (1-\eta_2)\Delta^2\hat{n}_3] - (1-\eta_1)(1-\eta_2)[\mathrm{Cov}(\hat{n}_2,\hat{n}_3)]^2}, \tag{F3}$$

leading us to the optimized symmetric single-parameter QFI

$$\mathcal{G}^{(ii)} = \frac{\eta_1\eta_2\langle\hat{n}_2\rangle\langle\hat{n}_3\rangle\mathcal{F}^{(ii)} + [\langle\hat{n}_2\rangle\eta_1(1-\eta_2) + \langle\hat{n}_3\rangle\eta_2(1-\eta_1)](\Delta^2\hat{n}_2\Delta^2\hat{n}_3 - \mathrm{Cov}(\hat{n}_2,\hat{n}_3)^2)}{\eta_1\eta_2\langle\hat{n}_2\rangle\langle\hat{n}_3\rangle + \eta_1(1-\eta_2)\langle\hat{n}_2\rangle\Delta^2\hat{n}_3 + (1-\eta_1)\eta_2\Delta^2\hat{n}_2\langle\hat{n}_3\rangle + (1-\eta_1)(1-\eta_2)(\Delta^2\hat{n}_2\Delta^2\hat{n}_3 - \mathrm{Cov}(\hat{n}_2,\hat{n}_3)^2)}, \tag{F4}$$

where $\mathcal{F}^{(ii)}$ is given by Eq. (18).

APPENDIX G: THE $\mathcal{A}$ COEFFICIENTS FOR THE EQUATION YIELDING THE OPTIMUM TRANSMISSION COEFFICIENT IN THE LOSSY SINGLE-PARAMETER QFI

For the input state obeying the constraint $\langle\hat{a}_0\rangle = 0$ implying $C_2' = C_4' = 0$, the optimum transmission coefficient of BS_1, $\vartheta_{\rm opt}^{(i)}$, is obtained by solving Eq. (62), and its $\mathcal{A}$ coefficients are as follows:

$$\begin{aligned} \mathcal{A}_4 &= \frac{(C_1')^2}{16}(1-\eta_2)\langle\hat{J}_z\rangle, \\ \mathcal{A}_3 &= C_1'\left(-\frac{C_3'}{2}(1-\eta_2) + 2\eta_2\langle\hat{J}_z\rangle\right)\langle\hat{J}_z\rangle, \\ \mathcal{A}_2 &= \left[\left(C_3'^2 - C_1'\frac{4C_0'+C_1'}{8}\right)(1-\eta_2) - \eta_2\frac{C_3'}{4}\langle\hat{J}_z\rangle - 2C_1'\eta_2\langle\hat{N}\rangle\right]\langle\hat{J}_z\rangle, \\ \mathcal{A}_1 &= C_3'\frac{4C_0'+C_1'}{2}(1-\eta_2)\langle\hat{J}_z\rangle + \frac{C_1'}{2}\eta_2\langle\hat{N}\rangle^2 + 4C_3'\eta_2\langle\hat{N}\rangle\langle\hat{J}_z\rangle, \\ \mathcal{A}_0 &= \frac{(4C_0'+C_1')^2}{16}(1-\eta_2)\langle\hat{J}_z\rangle - C_3'\eta_2\langle\hat{N}\rangle^2. \end{aligned} \tag{G1}$$

If we impose $\eta_2 \to 1$ to the previous results one has $\mathcal{A}_4 \to 0$ and Eq. (62) can be reformulated as $(C_1' \cos\vartheta - 2C_3')(\langle \hat{J}_z \rangle \cos\vartheta + \langle \hat{N} \rangle/2)^2 = 0$, leading to the obvious solution $\cos\vartheta = 2C_3'/C_1'$ which is actually the result from the lossless scenario [32] (see also the Supplemental Material [54]).

APPENDIX H: OPTIMUM TRANSMISSION COEFFICIENT FOR THE SYMMETRIC SINGLE-PARAMETER QFI

In the high-loss limit (i.e., $\eta_2 \ll 1 - \eta_1$) the optimum BS_1 transmission coefficient is found from the solutions of Eq. (65). Solving $\Delta^2 \hat{n}_3 + \mathrm{Cov}(\hat{n}_2, \hat{n}_3) = 0$ yields

$$t_\pm = -\frac{2\,\mathrm{Cov}(\hat{N}, \hat{J}_y) \mp \sqrt{4([\mathrm{Cov}(\hat{N}, \hat{J}_y)]^2 + [\mathrm{Cov}(\hat{N}, \hat{J}_z)]^2) - (\Delta^2 \hat{N})^2}}{\Delta^2 \hat{N} + 2\,\mathrm{Cov}(\hat{N}, \hat{J}_z)} \tag{H1}$$

and for $t_\pm \in \mathbb{R}$ one gets the optimum transmission coefficients $T_\pm^{(ii)} = \sqrt{[(1 - t_\pm^2)/[2(1 + t_\pm^2)]}$. Solving the equation $\mathrm{Cov}(\hat{n}_2, \hat{n}_3)(\Delta^2 \hat{n}_3)' + \Delta^2 \hat{n}_3 (\Delta^2 \hat{n}_2)' = 0$ in respect with the input fields results in the fourth-order equation

$$\mathcal{A}_c t^4 + \mathcal{B}_c t^3 + \mathcal{C}_c t^2 + \mathcal{D}_c t + \mathcal{E}_c = 0, \tag{H2}$$

where the coefficients are given by

$$\begin{aligned}
\mathcal{A}_c &= -2\,\mathrm{Cov}(\hat{N}, \hat{J}_z)\widehat{\mathrm{Cov}}(\hat{J}_y, \hat{J}_z) + 2\,\mathrm{Cov}(\hat{N}, \hat{J}_y)\Delta^2 \hat{J}_z + \mathrm{Cov}(\hat{N}, \hat{J}_y)\mathrm{Cov}(\hat{N}, \hat{J}_z) - \Delta^2 \hat{N}\widehat{\mathrm{Cov}}(\hat{J}_y, \hat{J}_z), \\
\mathcal{B}_c &= 4\,\mathrm{Cov}(\hat{N}, \hat{J}_y)\widehat{\mathrm{Cov}}(\hat{J}_y, \hat{J}_z) - 4\,\mathrm{Cov}(\hat{N}, \hat{J}_z)\Delta^2 \hat{J}_y - 2\Delta^2 \hat{N}(\Delta^2 \hat{J}_y - \Delta^2 \hat{J}_z) + 2[\mathrm{Cov}(\hat{N}, \hat{J}_y)]^2 - 2[\mathrm{Cov}(\hat{N}, \hat{J}_z)]^2, \\
\mathcal{C}_c &= -6\,\mathrm{Cov}(\hat{N}, \hat{J}_y)\mathrm{Cov}(\hat{N}, \hat{J}_z) + 6\Delta^2 \hat{N}\,\widehat{\mathrm{Cov}}(\hat{J}_y, \hat{J}_z), \\
\mathcal{D}_c &= 2\Delta^2 \hat{N}(\Delta^2 \hat{J}_y - \Delta^2 \hat{J}_z) - 2[\mathrm{Cov}(\hat{N}, \hat{J}_y)]^2 + 2[\mathrm{Cov}(\hat{N}, \hat{J}_z)]^2 + 4\,\mathrm{Cov}(\hat{N}, \hat{J}_y)\widehat{\mathrm{Cov}}(\hat{J}_y, \hat{J}_z) - 4\,\mathrm{Cov}(\hat{N}, \hat{J}_z)\Delta^2 \hat{J}_y, \\
\mathcal{E}_c &= 2\,\mathrm{Cov}(\hat{N}, \hat{J}_z)\widehat{\mathrm{Cov}}(\hat{J}_y, \hat{J}_z) - 2\,\mathrm{Cov}(\hat{N}, \hat{J}_y)\Delta^2 \hat{J}_z + \mathrm{Cov}(\hat{N}, \hat{J}_y)\mathrm{Cov}(\hat{N}, \hat{J}_z) - \Delta^2 \hat{N}\widehat{\mathrm{Cov}}(\hat{J}_y, \hat{J}_z).
\end{aligned} \tag{H3}$$

Equation (H2) leads to up to four solutions t_{sol}. Selecting the real ones among them, ones gets the BS_1 coefficients $T_{\mathrm{sol}}^{(ii)} = \sqrt{[(1 - t_{\mathrm{sol}}^2)/[2(1 + t_{\mathrm{sol}}^2)]}$. Replacing $T_\pm^{(ii)}$ and $T_{\mathrm{sol}}^{(ii)}$ in Eq. (38) allows one to select the actual solution $T_{\mathrm{opt}}^{(ii)}$ that maximizes the QFI.

For the simpler case when $\mathrm{Cov}(\hat{n}_2, \hat{n}_3) = 0$, Eq. (73) expressed in respect with the input field operators leads to the fourth-order equation

$$(\mathcal{B}_{\mathrm{sep}} - \mathcal{E}_{\mathrm{sep}})t_{\mathrm{sol}}^4 - 2(\mathcal{C}_{\mathrm{sep}} - \mathcal{D}_{\mathrm{sep}})t_{\mathrm{sol}}^3 + 2(2\mathcal{A}_{\mathrm{sep}} - \mathcal{B}_{\mathrm{sep}})t_{\mathrm{sol}}^2 + 2(\mathcal{C}_{\mathrm{sep}} + \mathcal{D}_{\mathrm{sep}})t_{\mathrm{sol}} + \mathcal{B}_{\mathrm{sep}} + \mathcal{E}_{\mathrm{sep}} = 0, \tag{H4}$$

where the coefficients are given by

$$\begin{aligned}
\mathcal{A}_{\mathrm{sep}} &= [(1 - \eta_2)\mathrm{Cov}(\hat{N}, \hat{J}_y) + 2\eta_2 \langle \hat{J}_y \rangle]\mathrm{Cov}(\hat{N}, \hat{J}_z) - \eta_2 \mathrm{Cov}(\hat{N}, \hat{J}_y)\langle \hat{J}_z \rangle, \\
\mathcal{B}_{\mathrm{sep}} &= -[(1 - \eta_2)\mathrm{Cov}(\hat{N}, \hat{J}_z) + 2\eta_2 \langle \hat{J}_z \rangle]\mathrm{Cov}(\hat{N}, \hat{J}_y) + \eta_2 \mathrm{Cov}(\hat{N}, \hat{J}_z)\langle \hat{J}_y \rangle, \\
\mathcal{C}_{\mathrm{sep}} &= [(1 - \eta_2)\mathrm{Cov}(\hat{N}, \hat{J}_y) + \eta_2 \langle \hat{J}_y \rangle]\mathrm{Cov}(\hat{N}, \hat{J}_y) - [(1 - \eta_2)\mathrm{Cov}(\hat{N}, \hat{J}_z) + \eta_2 \langle \hat{J}_z \rangle]\mathrm{Cov}(\hat{N}, \hat{J}_z), \\
\mathcal{D}_{\mathrm{sep}} &= \left((1 - \eta_2)\frac{\Delta^2 \hat{N}}{2} + \eta_2 \langle \hat{N} \rangle\right)\mathrm{Cov}(\hat{N}, \hat{J}_z) - \eta_2 \frac{\Delta^2 \hat{N}}{2}\langle \hat{J}_z \rangle, \\
\mathcal{E}_{\mathrm{sep}} &= \left((1 - \eta_2)\frac{\Delta^2 \hat{N}}{2} + \eta_2 \langle \hat{N} \rangle\right)\mathrm{Cov}(\hat{N}, \hat{J}_y) - \eta_2 \frac{\Delta^2 \hat{N}}{2}\langle \hat{J}_y \rangle.
\end{aligned} \tag{H5}$$

Among the solutions $\vartheta_{\mathrm{opt}}^{(ii)} = \arccos t_{\mathrm{sol}}$, one maximizes the two-parameter QFI, $\mathcal{G}^{(ii)}$.

In the general case, when differentiating the symmetric single-parameter QFI from Eq, (38) in respect with ϑ we get

$$\begin{aligned}
&\eta_2 \langle \hat{n}_3 \rangle [\mathrm{Cov}(\hat{n}_2, \hat{n}_3)' - \Delta^2 \hat{n}_3'] + (1 - \eta_2)(\eta_2 \langle \hat{n}_3 \rangle \Delta^2 \hat{n}_3 (3\Delta^2 \hat{n}_2' + \Delta^2 \hat{n}_3') + [\Delta^2 \hat{n}_3]^2 [\eta_2 \langle \hat{n}_3 \rangle' + (1 - \eta_2)\Delta^2 \hat{n}_2') \\
&- 2\,\mathrm{Cov}(\hat{n}_2, \hat{n}_3)\Delta^2 \hat{n}_3 (\eta_2 \langle \hat{n}_3 \rangle' + (1 - \eta_2)\mathrm{Cov}(\hat{n}_2, \hat{n}_3)'] + [\mathrm{Cov}(\hat{n}_2, \hat{n}_3)]^2 [\eta_2 \langle \hat{n}_3 \rangle' + (1 - \eta_2)\Delta^2 \hat{n}_3']) = 0
\end{aligned} \tag{H6}$$

and by employing Eqs. (6) and (A1) we are able to rewrite Eq. (H6) in respect with ϑ. Following a process similar to the one described in the Supplemental Material [54], one is able to find the solution ϑ_{opt} that maximizes the QFI from Eq. (38).

APPENDIX I: DOUBLE COHERENT INPUT STATE

Considering a double coherent input state, for the scenario having no access to an external phase reference we find the two-parameter QFI

$$\mathcal{G}^{(2p)} = \frac{2\eta_2 |\alpha|^2 [1 + \varpi^2 - (\varpi^2 - 1)\cos\vartheta + 2\varpi\,\sin\vartheta\,\sin\Delta\theta][1 + \varpi^2 + (\varpi^2 - 1)\cos\vartheta - 2\varpi\,\sin\vartheta\,\sin\Delta\theta]}{(1 + \eta_2)(\varpi^2 + 1) + (1 - \eta_2)(\varpi^2 - 1)\cos\vartheta - 2(1 - \eta_2)\varpi \sin\vartheta \sin\Delta\theta}. \tag{I1}$$

Solving Eq. (54) and taking into account that for any coherent state we have the constraint $\Delta^2\hat{n}_l = \langle\hat{n}_l\rangle$, where l denotes the mode, we arrive at the result

$$\vartheta_{\rm opt}^{(2p)} = 2\ \arctan\frac{(1+\sqrt{\eta_2})\Big(\varpi\ \sin\Delta\theta + {\rm sign}(1-\varpi)\sqrt{\varpi^2\sin^2\Delta\theta + \frac{(1-\sqrt{\eta_2}\varpi^2)(\sqrt{\eta_2}-\varpi^2)}{(1+\sqrt{\eta_2})^2}}\Big)}{1-\sqrt{\eta_2}\varpi^2} \tag{I2}$$

and the optimum transmission coefficient is found via Eq. (76).

For the symmetric single-parameter lossy QFI the result from Eq. (82) expanded yields

$$\mathcal{G}^{(ii)} = \frac{|\alpha|^2}{2}\{(1+\eta_2)(1+\varpi^2) - (1-\eta_2)[2\ \sin\vartheta\varpi\ \sin\Delta\theta + \cos\vartheta(1-\varpi^2)]\} \tag{I3}$$

and its maximum is reached in the degenerate case $T_{\rm opt}^{(ii)} = [1-{\rm sign}(\varpi-1)]/2$ if $\sin\Delta\theta \geqslant 0$ and for

$$T_{\rm opt}^{(ii)} = \sqrt{\frac{1}{2} + \frac{(1-\varpi^2){\rm sign}(1-\varpi)}{2\sqrt{4\varpi^2\sin^2\Delta\theta + (1-\varpi^2)^2}}}, \tag{I4}$$

otherwise, leading to the maximum QFI

$$\mathcal{G}_{\rm max}^{(ii)} = \frac{|\alpha|^2}{2}((1-\eta_2)\sqrt{4\varpi^2\sin^2\Delta\theta + (1-\varpi^2)^2} + (1+\eta_2)(1+\varpi^2)). \tag{I5}$$

APPENDIX J: CALCULATIONS FOR THE COHERENT PLUS SQUEEZED VACUUM INPUT STATE

In the high-coherent regime (i.e., $|\alpha|^2 \gg \sinh^2 r$), one finds $\cos\vartheta_{\rm opt}^{(i)} \approx 1 + \frac{e^{-r}-\sqrt{\eta_2-\eta_2^2(1-e^{-2r})}}{(1-\eta_2)\sinh r}$ from the QFI given by Eq. (96), a result valid for $\eta_2 < 1$, and it implies the optimum transmission coefficient

$$T_{\rm opt}^{(i)} \approx \sqrt{1 + \frac{e^{-r} - \sqrt{\eta_2 - \eta_2^2(1-e^{-2r})}}{2(1-\eta_2)\sinh r}}, \tag{J1}$$

leading to the maximum asymmetric single-parameter QFI

$$\mathcal{G}_{\rm max}^{(i)} \approx \frac{2|\alpha|^2\eta_2(e^r + \eta_2 e^{-r} - 2\eta_2\sinh r - 2\sqrt{\eta_2 + \eta_2^2(1-e^{-2r})})}{\sinh r(1-\eta_2)^2}. \tag{J2}$$

The single-parameter symmetric lossy QFI is maximized by employing the optimum BS_1 transmission coefficient from Eq. (99), a result valid in the high-coherent approximation. One ends up with the maximum symmetric single-parameter lossy QFI

$$\mathcal{G}_{\rm max}^{(ii)} = \frac{|\alpha|^2[(1-\eta_2)(3\eta_2+1)e^{2r} - 4(1+\eta_2)(\sqrt{\eta_2 e^r(e^r - 2\eta_2\sinh r)} - \eta_2)]}{(e^{2r}-1)(1-\eta_2)^2}. \tag{J3}$$

APPENDIX K: CALCULATIONS FOR THE COHERENT PLUS FOCK INPUT STATE

By employing Eqs. (27), (101), and (103) we find the optimized two-parameter QFI

$$\mathcal{G}^{(2p)} = \frac{2\eta_2(|\alpha|^2 + 2|\alpha|^2 n + n)\sin^2\vartheta[|\alpha|^2 + (|\alpha|^2 - n)\cos\vartheta + n]}{(1-\eta_2)(|\alpha|^2 + 2|\alpha|^2 n + n)\sin^2\vartheta + 2\eta_2[|\alpha|^2 + (|\alpha|^2 - n)\cos\vartheta + n]}. \tag{K1}$$

The optimum BS_1 transmission coefficient maximizing the two-parameter QFI is found among the solutions of equation

$$B_{\rm cf}C_{\rm cf}x^4 - 2B_{\rm cf}^2x^3 - 2B_{\rm cf}(2A_{\rm cf} + C_{\rm cf})x^2 - 2A_{\rm cf}^2x + B_{\rm cf}C_{\rm cf} = 0, \tag{K2}$$

where $\vartheta = \arccos(x)$ and the coefficients of the previous equation are given by

$$\begin{aligned} A_{\rm cf} &= 2\eta_2(|\alpha|^2 + n), \\ B_{\rm cf} &= 2\eta_2(|\alpha|^2 - n), \\ C_{\rm cf} &= (1-\eta_2)(|\alpha|^2 + 2|\alpha|^2 n + n). \end{aligned} \tag{K3}$$

In the high-coherent approximation ($|\alpha|^2 \gg n$) the QFI $\mathcal{G}^{(ii)}$ can be approximated to

$$\mathcal{G}^{(ii)} \approx \frac{|\alpha|^2\{(2n+1)[1-(1-\eta_2)\cos\vartheta] + (1-2n\cos2\vartheta)\eta_2\}}{2[(1-\eta_2)n(1-\cos\vartheta) + 1]} \tag{K4}$$

and maximizing this expression in respect with the parameter ϑ yields the optimum BS_1 transmission coefficient given in Eq. (111). Replacing this value into Eq. (K4) leads us to the maximum QFI

$$\mathcal{G}^{(ii)}_{\max} \approx \frac{|\alpha|^2\left(\eta_2^2(1-6n)+2\eta_2(3+2n)-4(1+\eta_2)\sqrt{\eta_2[1+2n(1-\eta_2)]}+2n+1\right)}{2(1-\eta_2)^2 n}. \tag{K5}$$

APPENDIX L: TWIN FOCK INPUT

While optimizing in respect with ϑ in Eq. (115) one gets the fourth-order equation

$$(1-\eta_2)(m+n+2mn)y^4+4\eta_2(m-n)y^3-2[(1-\eta_2)(m+n+2mn)+4\eta_2(m+n)]y^2 + 4\eta_2\frac{(m+n)^2}{m-n}y+(1-\eta_2)(m+n+2mn)=0 \tag{L1}$$

valid for $m \neq n$ and $\vartheta = \arccos y$. Among the solutions ϑ_{sol} of the previous equation, one maximizes the QFI from Eq. (115).

[1] V. Giovannetti, S. Lloyd, and L. Maccone, Science **306**, 1330 (2004).
[2] V. Giovannetti, S. Lloyd, and L. Maccone, Phys. Rev. Lett. **96**, 010401 (2006).
[3] J. P. Dowling and K. P. Seshadreesan, J. Lightwave Technol. **33**, 2359 (2015).
[4] C. L. Degen, F. Reinhard, and P. Cappellaro, Rev. Mod. Phys. **89**, 035002 (2017).
[5] H. Grote, K. Danzmann, K. L. Dooley, R. Schnabel, J. Slutsky, and H. Vahlbruch, Phys. Rev. Lett. **110**, 181101 (2013).
[6] R. Schnabel, Phys. Rep. **684**, 1 (2017).
[7] M. Tse *et al.*, Phys. Rev. Lett. **123**, 231107 (2019).
[8] F. Acernese *et al.*(Virgo Collaboration), Phys. Rev. Lett. **131**, 041403 (2023).
[9] D. Ganapathy *et al.* (LIGO O4 Detector Collaboration), Phys. Rev. X **13**, 041021 (2023).
[10] M. A. Taylor, J. Janousek, V. Daria, J. Knittel, B. Hage, H.-A. Bachor, and W. P. Bowen, Nat. Photon. **7**, 229 (2013).
[11] M. A. Taylor and W. P. Bowen, Phys. Rep. **615**, 1 (2016).
[12] Z. He, Y. Zhang, X. Tong, L. Li, and L. V. Wang, Nat. Commun. **14**, 2441 (2023).
[13] L. Pezzé and A. Smerzi, Phys. Rev. A **73**, 011801(R) (2006).
[14] R. Demkowicz-Dobrzański, M. Jarzyna, and J. Kołodyński, Prog. Opt. **60**, 345 (2015).
[15] B. T. Gard, C. You, D. K. Mishra, R. Singh, H. Lee, T. R. Corbitt, and J. P. Dowling, EPJ Quantum Technol. **4**, 4 (2017).
[16] K. K. Mishra and S. Ataman, Phys. Rev. A **106**, 023716 (2022).
[17] R. A. Fisher, Proc. R. Soc. Edinb. **42**, 321 (1923).
[18] S. L. Braunstein, Phys. Rev. Lett. **69**, 3598 (1992).
[19] S. L. Braunstein and C. M. Caves, Phys. Rev. Lett. **72**, 3439 (1994).
[20] W. Zhong, Y. Huang, X. Wang, and S.-L. Zhu, Phys. Rev. A **95**, 052304 (2017).
[21] W. Zhong, L. Zhou, and Y.-B. Sheng, Phys. Rev. A **103**, 042611 (2021).
[22] M. Fréchet, Rev. Inst. Int. Statist. **11**, 182 (1943).
[23] C. R. Rao, Bull. Calcutta Math. Soc. **37**, 81 (1945).
[24] H. Cramér, *Mathematical Methods of Statistics* (Princeton University Press, Princeton, NJ, 1946).
[25] C. Helstrom, Phys. Lett. A **25**, 101 (1967).
[26] C. Helstrom, IEEE Trans. Inf. Theory **14**, 234 (1968).
[27] M. G. A. Paris, Int. J. Quantum Inf. **07**, 125 (2009).
[28] J. Liu, H. Yuan, X.-M. Lu, and X. Wang, J. Phys. A: Math. Theor. **53**, 023001 (2020).
[29] M. Jarzyna and R. Demkowicz-Dobrzański, Phys. Rev. A **85**, 011801(R) (2012).
[30] W. Zhong, P. Xu, and Y. Sheng, Sci. China Phys. Mech. Astron. **63**, 260312 (2020).
[31] S. Ataman, Phys. Rev. A **102**, 013704 (2020).
[32] S. Ataman, Phys. Rev. A **105**, 012604 (2022).
[33] J.-D. Zhang and S. Wang, Phys. Rev. A **107**, 043704 (2023).
[34] J. Kołodyński and R. Demkowicz-Dobrzański, Phys. Rev. A **82**, 053804 (2010).
[35] M. Kacprowicz, R. Demkowicz-Dobrzanski, W. Wasilewski, K. Banaszek, and I. A. Walmsley, Nat. Photon. **4**, 357 (2010).
[36] S. Knysh, V. N. Smelyanskiy, and G. A. Durkin, Phys. Rev. A **83**, 021804(R) (2011).
[37] J. J. Cooper and J. A. Dunningham, New J. Phys. **13**, 115003 (2011).
[38] A. B. Klimov, M. Zwierz, S. Wallentowitz, M. Jarzyna, and K. Banaszek, New J. Phys. **19**, 073013 (2017).
[39] T. Ono and H. F. Hofmann, Phys. Rev. A **81**, 033819 (2010).
[40] C. Oh, S.-Y. Lee, H. Nha, and H. Jeong, Phys. Rev. A **96**, 062304 (2017).
[41] P. M. Anisimov, G. M. Raterman, A. Chiruvelli, W. N. Plick, S. D. Huver, H. Lee, and J. P. Dowling, Phys. Rev. Lett. **104**, 103602 (2010).
[42] W. Huang, X. Liang, C.-H. Yuan, W. Zhang, and L. Chen, Results Phys. **50**, 106574 (2023).
[43] S.-Y. Lee, Y. S. Ihn, and Z. Kim, Phys. Rev. A **101**, 012332 (2020).
[44] X.-X. Zhang, Y.-X. Yang, and X.-B. Wang, Phys. Rev. A **88**, 013838 (2013).
[45] W. Huang, X. Liang, B. Zhu, Y. Yan, C.-H. Yuan, W. Zhang, and L. Q. Chen, Phys. Rev. Lett. **130**, 073601 (2023).
[46] M. Takeoka, K. P. Seshadreesan, C. You, S. Izumi, and J. P. Dowling, Phys. Rev. A **96**, 052118 (2017).
[47] D. Gatto, P. Facchi, and V. Tamma, Int. J. Quantum Inf. **18**, 1941019 (2020).
[48] X. Yu, X. Zhao, L. Shen, Y. Shao, J. Liu, and X. Wang, Opt. Express **26**, 16292 (2018).
[49] J. Liu, M. Zhang, H. Chen, L. Wang, and H. Yuan, Adv. Quantum Technol. **5**, 2100080 (2022).

[50] B. M. Escher, R. L. de Matos Filho, and L. Davidovich, Nat. Phys. **7**, 406 (2011).
[51] B. Yurke, S. L. McCall, and J. R. Klauder, Phys. Rev. A **33**, 4033 (1986).
[52] C. Gerry and P. Knight, *Introductory Quantum Optics* (Cambridge University Press, Cambridge, 2005).
[53] M. D. Lang and C. M. Caves, Phys. Rev. Lett. **111**, 173601 (2013).
[54] See Supplemental Material at http://link.aps.org/supplemental/10.1103/PhysRevA.109.062605 for more detail the lossless case and also provide the full calculation for the solution to Eq. (64).
[55] B. M. Escher, R. L. de Matos Filho, and L. Davidovich, Braz. J. Phys **41**, 229 (2011).
[56] R. Demkowicz-Dobrzanski, U. Dorner, B. J. Smith, J. S. Lundeen, W. Wasilewski, K. Banaszek, and I. A. Walmsley, Phys. Rev. A **80**, 013825 (2009).
[57] U. Dorner, R. Demkowicz-Dobrzanski, B. J. Smith, J. S. Lundeen, W. Wasilewski, K. Banaszek, and I. A. Walmsley, Phys. Rev. Lett. **102**, 040403 (2009).
[58] J.-T. Shin, H.-N. Kim, G.-D. Park, T.-S. Kim, and D.-Y. Park, J. Opt. Soc. Korea **3**, 1 (1999).
[59] A. Preda and S. Ataman, Phys. Rev. A **99**, 053810 (2019).
[60] L. Pezzé and A. Smerzi, Phys. Rev. Lett. **100**, 073601 (2008).
[61] A. I. Lvovsky and S. A. Babichev, Phys. Rev. A **66**, 011801(R) (2002).
[62] R. Birrittella, J. Mimih, and C. C. Gerry, Phys. Rev. A **86**, 063828 (2012).
[63] R. J. Birrittella, P. M. Alsing, and C. C. Gerry, AVS Quantum Sci. **3**, 014701 (2021).
[64] M. J. Holland and K. Burnett, Phys. Rev. Lett. **71**, 1355 (1993).
[65] Z. Huang, K. R. Motes, P. M. Anisimov, J. P. Dowling, and D. W. Berry, Phys. Rev. A **95**, 053837 (2017).
[66] S. L. Braunstein and P. van Loock, Rev. Mod. Phys. **77**, 513 (2005).
[67] K. Fukui and S. Takeda, J. Phys. B: At. Mol. Opt. Phys. **55**, 012001 (2022).
[68] L. Mandel and E. Wolf, *Optical Coherence and Quantum Optics* (Cambridge University Press, Cambridge, 1995).
[69] G. S. Agarwal, *Quantum Optics* (Cambridge University Press, Cambridge, 2012).
[70] C. M. Caves, Phys. Rev. D **23**, 1693 (1981).
[71] S. Ataman, A. Preda, and R. Ionicioiu, Phys. Rev. A **98**, 043856 (2018).
[72] L. Pezzé and A. Smerzi, Phys. Rev. Lett. **110**, 163604 (2013).
[73] R. A. Campos, C. C. Gerry, and A. Benmoussa, Phys. Rev. A **68**, 023810 (2003).
[74] J. Zeng, D. Li, L. Q. Chen, W. Zhang, and C.-H. Yuan, arXiv:2302.09823.
[75] S. Ataman, Eur. Phys. J. D **76**, 233 (2022).